Noise-affected I-V curves in small hysteretic Josephson junctions

R. L. Kautz and John M. Martinis
National Institute of Standards and Technology, 325 Broadway, Boulder, Colorado 80303-3328
(Received 11 June 1990)

We investigate the noise-affected I-V curves of small-area Josephson junctions through experiment, simulation, and theory. In particular, we consider I-V curves in which two different states of finite voltage coexist at the same dc bias: a high-voltage state that corresponds to the usual quasiparticle branch and a low-voltage state that is characterized by thermally activated phase diffusion. The observed hysteresis between the phase-diffusion and quasiparticle branches cannot be explained within the context of the simple resistively and capacitively shunted junction (RCSJ) model but is explained by extended models in which the damping increases with frequency. Frequency-dependent damping is shown to produce a qualitative change in the attractors of the noise-free system which allows the two voltage states to be simultaneously stable. This picture is confirmed by Monte Carlo simulations which accurately reproduce the experimental I-V curves of two different samples over a wide range of temperatures. In addition we develop analytic expressions for three key parameters of the I-V curve of junctions displaying hysteresis between the phase-diffusion and quasiparticle branches: the initial slope of the phase-diffusion branch, the bias level at which the junction switches from the phase-diffusion branch to the quasiparticle branch, and the bias level at which it returns to the phase-diffusion branch.

I. INTRODUCTION

In the exploration of effects associated with single-electron tunneling in Josephson junctions, many investigators have recently fabricated junctions of small area for which the Josephson coupling energy $E_J=\hbar I_0/2e$ is on the order of the charging energy $E_C=e^2/2C$ (where I_0 is the ideal critical current and C is the capacitance of the junction). For such junctions the critical current is often in the nanoampere range, the capacitance is measured in femtofarads, and the subgap resistance can be many megohms. Several experimental studies of this type of junction have revealed a new kind of current-voltage (I-V) characteristic that exhibits both hysteresis and a small voltage associated with the nominal zero-voltage branch.[1-6]

An example of an I-V curve with these properties is shown at three different scales in Fig. 1 for a small-area $Nb/NbO_x/Pb$-In-Au tunnel junction. Frame (a) of Fig. 1 is an overview showing the expected current rise at the energy-gap voltage near 2.8 mV. In this case the current rise is about 70 nA, implying an ideal critical current of roughly 50 nA. While a critical current of this magnitude is not observed, at dc-bias levels below 1.2 nA there is a low-voltage branch that overlaps the usual quasiparticle branch at higher voltages. This region of hysteresis is shown in Fig. 1(b) at an expanded current scale but the same voltage scale as Fig. 1(a). If the low-voltage branch were actually at zero voltage as Fig. 1(b) suggests, then the I-V curve could be explained as one in which the critical current is suppressed below its ideal value by thermal noise, a common situation in hysteretic junctions. However, when the voltage scale is expanded as in Fig. 1(c), the low-voltage branch is found to be at finite voltage and have a finite slope even at zero dc bias. Although a finite slope at zero bias is often observed in nonhysteretic I-V curves in the presence of noise, it is unusual in an I-V curve displaying hysteresis.

Because the type of I-V curve shown in Fig. 1 is observed in junctions for which E_J is on the order of E_C, processes involving single-electron tunneling (SET) or macroscopic quantum tunneling (MQT) can be important determining factors. Indeed, valuable information about such processes has been obtained by studying I-V curves of this type.[3-5] However, the characteristics of hysteresis and a finite slope at the origin have also been observed, as in Fig. 1, in junctions for which E_J is much larger than E_C and processes beyond the classical dynamics of Josephson junctions can be excluded. In this paper, we restrict our attention to this classical regime ($E_J \gg E_C$) and seek to understand I-V curves of the type shown in Fig. 1 in terms of the Josephson equations and thermal noise.

Although a hysteretic I-V curve with a finite slope at the origin does not necessarily imply the presence of SET or MQT processes, an explanation within the simplest classical model of junction dynamics, the resistivity and capacitively shunted junction (RCSJ) model of Stewart[7] and McCumber,[8] is not believed to be possible. As was first noted by Ono *et al.*,[2] the characteristic shown in Fig. 1 combines features expected of the noise-affected I-V curves of hysteretic (underdamped) and nonhysteretic (overdamped) junctions within the RCSJ model. In the overdamped case, the junction voltage is necessarily zero at dc bias levels I less than the critical current I_0 in the absence of noise. In the presence of noise, the junction phase is subject to a diffusion process that gives rise to finite voltages for $|I|<I_0$ and, at sufficiently high noise levels, to a finite slope at the origin of the I-V curve. Phase-diffusion in overdamped junctions has been ana-

lyzed within the RCSJ model and the predictions[9] are in good agreement with experiment.[10] Such phase diffusion would explain the finite slope at the origin of the I-V curve shown in Fig. 1. In the underdamped case, there is a range of dc bias, $I_{r0} < |I| < I_0$, for which two different states of the junction, one at zero voltage and one at a finite voltage, are stable in the absence of noise. When the effect of noise on this hysteretic situation was first considered within the RCSJ model,[11] it was assumed that noise would cause the junction to switch from the zero-voltage state to the voltage state without producing the phase diffusion that would give a small voltage to the nominal zero-voltage state. Subsequent experiments have confirmed this assumption,[12] and Ono *et al.*[2] have argued that it is impossible to obtain phase diffusion in a hysteretic I-V curve within the RCSJ model. Phase diffusion is possible in the underdamped RCSJ model but it occurs only at low bias levels (roughly $|I| < I_{r0}$) and at temperatures high enough that the I-V curve does not display hysteresis. Thus, the RCSJ model is believed to explain both hysteresis and phase diffusion but not their simultaneous presence in a single I-V curve. In this paper, we present further arguments in support of this conclusion.

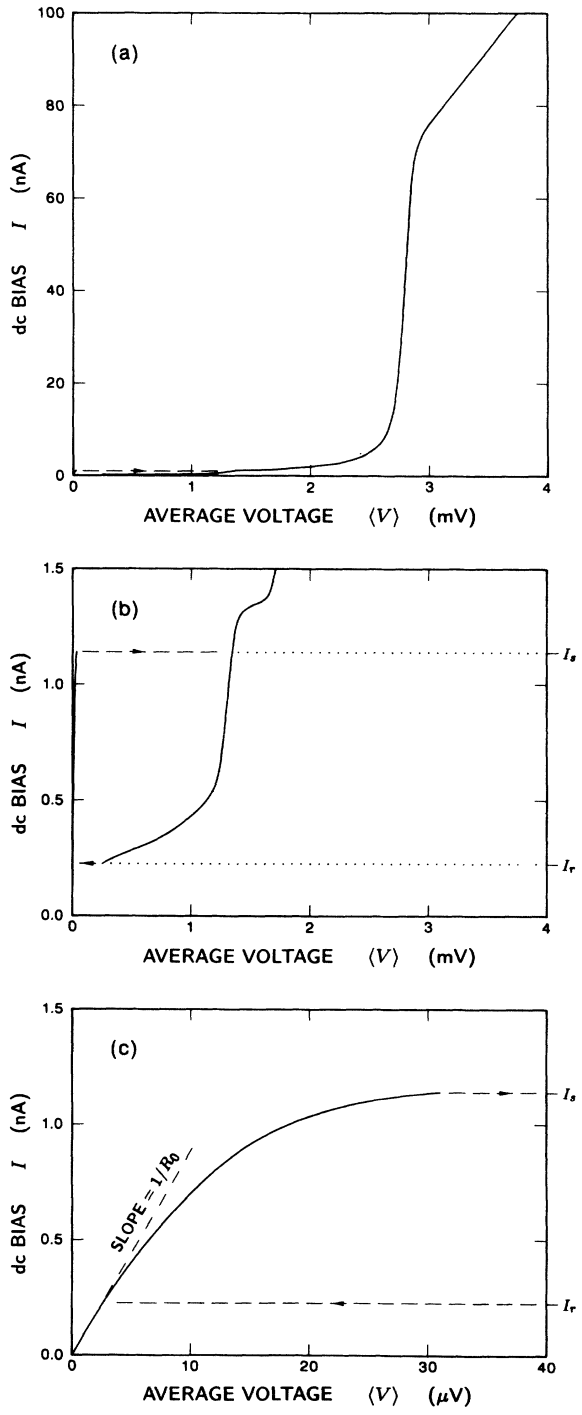

FIG. 1. The current-voltage characteristic of a $Nb/NbO_x/Pb$-In-Au tunnel junction measuring 0.1 by 1 μm^2 (sample B) at a temperature of 2.9 K.

A model that satisfactorily explains the type of I-V curve shown in Fig. 1 in terms of classical junction dynamics was first proposed by Ono *et al.*[2] Taking note of the fact that phase diffusion near zero voltage is stabilized by high damping and that an overlapping high-voltage state is stabilized by low damping, these authors suggested than an I-V characteristic displaying both phase diffusion and hysteresis might result if the damping were frequency dependent. Because phase diffusion involves motion at or near the junction's plasma frequency $\omega_p = \sqrt{2eI_0/\hbar C}$ and the voltage state involves primarily steady motion, the required frequency dependence is one that gives high damping near ω_p and low damping at zero frequency. Moreover, as Ono *et al.* point out, just this kind of damping profile can be expected in experiments with junctions having high subgap resistances. The required frequency dependence is not intrinsic to the junction but results because the leads attached to record the I-V curve shunt the junction with what can be characterized as a transmission line having a characteristic impedance on the order of or less than the impedance of free space, 377 Ω. At low frequencies, this transmission line merely connects the junction to a high-impedance current source and/or amplifier and the effective shunt resistance can be as high as the intrinsic resistance of the junction. At microwave frequencies, however, the effective shunt will be limited to a resistance no larger than the characteristic impedance of the transmission line. If the junction's intrinsic resistance is much higher than this characteristic impedance, we obtain a situation in which the damping is low at zero frequency and high at microwave frequencies. According to this picture, the type of I-V curve shown in Fig. 1 is likely to be obtained in the presence of noise whenever the subgap resistance is much greater than the impedance of free space.

Simulations reported by Ono *et al.*[2] confirm that frequency-dependent damping allows the coexistence of phase diffusion and hysteresis in a single I-V curve. However, because the external impedance shunting the junction was not well known at microwave frequencies in this and other early experiments,[1-5] the analysis was necessarily incomplete and largely qualitative. More recently, we measured I-V curves such as that shown in Fig. 1 using an experimental arrangement which allows an accurate characterization of the damping at microwave frequencies and obtained, for the first time, de-

tailed quantitative agreement between simulation and experiment.[6] This work established that phase diffusion in hysteretic junctions can be adequately described by an extended RCSJ model that includes frequency-dependent damping.

In the present paper, we expand on our earlier work,[6] describing the experiments and simulations at greater length and presenting in addition analytic results that provide insight into the nature of the phase-diffusion state. We focus on predicting the three parameters of the *I-V* curve identified in Fig. 1(c): the bias current I_s at which the junction switches from the phase-diffusion state to the voltage state, the bias current I_r at which the junction returns to the phase-diffusion state, and the resistance R_0 that characterizes the initial slope of the *I-V* curve. We consider the behavior of these parameters for three circuits that range in complexity from the basic RCSJ model, Fig. 2(a), to an extended RCSJ model with a simple frequency-dependent shunt, Fig. 2(b), to an extended RCSJ model that corresponds to our experiment, Fig. 2(c). We show that there is a qualitative difference between the circuits of Figs. 2(a) and 2(b) that allows the coexistence of phase diffusion and hysteresis in the latter case. We also show that the three parameters, I_s, I_r, and R_0, all depend, to varying degrees, on damping near the plasma frequency.

As the above discussion indicates, it is important to control the external shunting impedance at microwave frequencies in experiments with junctions having a high internal resistance. In our experiment this was achieved by including two isolation resistors on the microcircuit with the junction, as shown in Fig. 3. In the two samples studied, the junctions were virtually identical but the isolation resistors were purposely different. In sample A these resistors were 1.5 mm long with a resistance of 300 kΩ and in sample B they were 0.5 mm long with a resistance of 100 kΩ. Because the isolation resistors were made to be small compared with the wavelength of radiation at the plasma frequency, it was originally assumed that the shunting impedance at this frequency could not be less than the parallel combination of the two resistors, 150 kΩ for sample A and 50 kΩ for sample B. However, while trying to understand our experimental results, we learned that it is necessary to include the effect of a small distributed capacitance between the isolation resistors and the ground connection of the microcircuit. At high frequencies, this parasitic capacitance effectively grounds the isolation resistors at some point along their length, making their high-frequency resistance much less than the dc value. Only when this parasitic capacitance was accounted for did we obtain satisfactory agreement between simulation and experiment.

The phase-diffusion branch of the *I-V* curve is plotted in Fig. 4 for samples A and B at each of three temperatures. In this figure, solid lines show the experimental results and circles, squares, and rectangles show the results of Monte Carlo simulations based on the circuit model of Fig. 2(c). The agreement between simulation and experiment displayed here is remarkable given that all parameters entering the simulation were either experimentally measured or estimated from the sample geometry. Only

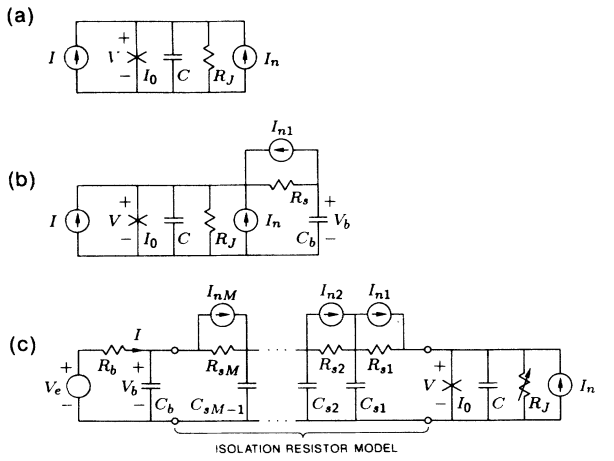

FIG. 2. Circuits for which noise-affected *I-V* curves are calculated: (a) the basic RCSJ model, (b) the RCSJ model with a simple frequency-dependent shunt, and (c) the circuit model for our experiment.

one circuit parameter, the ideal critical current I_0, was adjusted to fit the experimental phase-diffusion curves and the resulting value of 50 nA is consistent with the observed 70-nA step at the energy gap. The final quantitative agreement between simulation and experiment shown in Fig. 4 leaves little doubt that our circuit model captures the essential physics of phase diffusion in hysteretic *I-V* curves. We are thus confident that the complex dynamics of the phase-diffusion process recorded in our Monte Carlo simulations represents the real dynamics of noise-affected junctions.

By way of further introduction, we now briefly examine the dynamics of phase diffusion as revealed in our Monte Carlo simulations. The basic nature of phase diffusion is most easily understood in terms of the RCSJ model. Within this model, phase diffusion is equivalent to the Brownian motion of a particle in a potential of the form,

$$U(\phi) = -E_J[\cos\phi + (I/I_0)\phi] , \tag{1}$$

where ϕ is the difference in the superconducting phase across the junction. This potential has the shape of a washboard with a tilt determined by I and, for $|I| < I_0$,

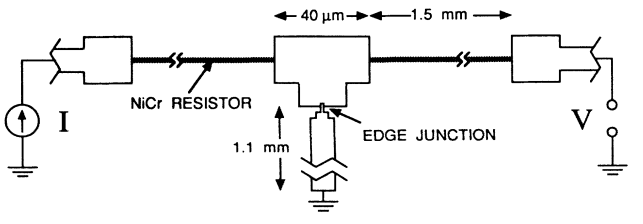

FIG. 3. Physical layout of the sample-A microcircuit consisting of a Nb/NbO_x/Pb-In-Au edge junction measuring 0.1 by 1 μm^2 and two NiCr resistors that are 4.5 nm thick, 1.5 μm wide, and 1.5 mm long fabricated on a silicon substrate. Sample B is similar but has resistors 0.5 mm long.

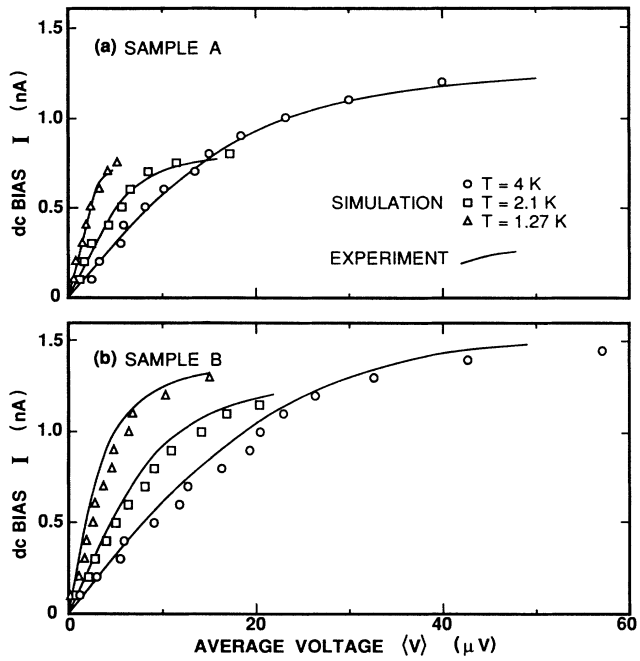

FIG. 4. Phase-diffusion branch of the I-V curve for (a) sample A and (b) sample B. Circles, squares, and triangles show simulated results at three temperatures based on average voltages computed over a time of 10 μs. Solid lines show corresponding experimental results. The upper limit of each curve defines the switching current I_s.

has local minima evenly spaced at 2π intervals in ϕ. Phase diffusion proceeds as a random walk among these equilibrium positions driven by the Johnson noise of the junction resistance. For nonzero I, phase diffusion leads to an average voltage,

$$\langle V \rangle = \frac{\hbar}{2e} \langle d\phi/dt \rangle \ , \tag{2}$$

because the tilt of the potential makes thermally induced escape from a minimum more probable in one direction than the other.

Extending the RCSJ model to include frequency-dependent damping does not significantly change this picture of phase diffusion: it simply allows the coexistence of phase diffusion and hysteresis in the same I-V curve. Consider, for example, phase diffusion at $I=0.5$ nA for the experimental I-V curve shown in Fig. 1(c). A Monte Carlo simulation for this case reveals the noise-affected dynamics of the junction phase and voltage shown in Fig. 5. Here, the phase is plotted over a range that includes three oscillations of the potential, with potential minima occurring near $\phi=-2\pi$, 0, and 2π and maxima near $\phi=-\pi$ and π. Whenever the phase drifts outside of this range it is renormalized by adding or subtracting 6π to restore numerical values to the plotting area. If there were no noise in the circuit, the phase would remain forever at a given minimum of the potential. In the presence of noise, the phase is continually buffeted and executes a random walk that is strongly affected by the potential. For significant periods of time, the phase remains trapped

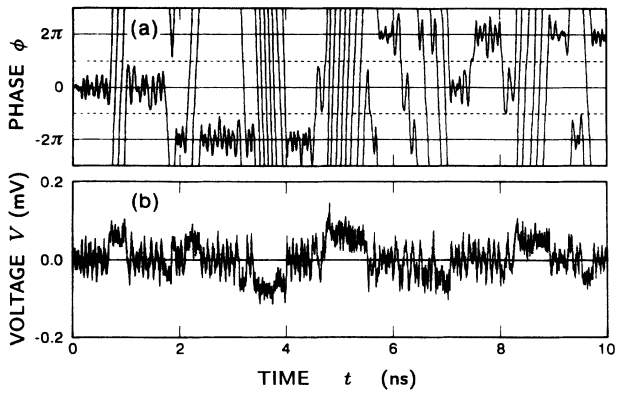

FIG. 5. Time dependence of (a) the phase and (b) the voltage of a junction in the phase-diffusion state as calculated in a Monte Carlo simulation. The simulation corresponds to the experimental situation shown in Fig. 1 for a dc bias of $I=0.5$ nA.

in one of the potential wells and oscillates about the potential minimum at roughly the plasma frequency. Occasionally, these oscillations build to the point where escape occurs and the phase begins to traverse the washboard, often moving across several minima before retrapping. Because $I/I_0=0.01$ in the present case, the tilt of the washboard is slight and these escape events produce motion in the $-\phi$ direction almost as often as in the $+\phi$ direction. Thus, although the phase moves in fits and starts, the general character of its motion is that of a random walk.

As Fig. 1 shows, there is, at $I=0.5$ nA, an ordinary voltage state near 1.1 mV on the quasiparticle branch of the characteristic in addition to the phase-diffusion state near 6.5 μV. The Monte Carlo simulations reproduce both of these states and show that they are distinct. That is, although the junction might be said to enter a voltage state when the phase escapes from a potential well in the phase-diffusion process, Fig. 5(b) shows that the voltages attained in these escape events are typically no more than one tenth of the voltage associated with the quasiparticle branch. Thus, the behavior shown in Fig. 5 cannot be interpreted as one in which the junction switches rapidly back and forth between the zero-voltage state and the quasiparticle branch. Instead, the low-voltage state of the phase-diffusion branch and the high-voltage state of the quasiparticle branch are independent and simultaneously stable, although they are both states in which the phase moves down the slope of the washboard potential. The simultaneous stability of these two states depends on the fact that the damping is frequency dependent.

Another significant feature of the phase-diffusion process shown in Fig. 5 is the prevalence of escape events in which the phase traverses many potential minima before retrapping. In the traditional analysis of phase diffusion in underdamped junctions,[13,14] which is valid in the limit of low temperature, it is assumed that escape always leads to a single 2π phase slip. This assumption is not valid in the present experiment because of the relatively high temperatures involved. To account for the multiple-well phase-slip events observed in Fig. 5, we have extended the traditional analysis to include a probability distribu-

tion for the number of wells traversed. This analysis yields a formula for the initial slope of the phase-diffusion branch of the I-V curve is in good agreement with Monte Carlo simulations for all three of the circuit models considered. Thus, we report new results not only for the case of frequency-dependent damping but also for the high-temperature limit of the much-studied RCSJ model.

The remainder of this paper is outlined as follows. In Sec. II we review the effect of noise within the RCSJ model and report the first accurate computation of the dc bias at which the stability of the zero-voltage and voltage states are equal. In Sec. III we introduce a simple extension of the RCSJ model that includes frequency-dependent damping and show that the basins of attraction for this system are topologically different from those of the RCSJ model. In Sec. IV we discuss our experiment and develop a circuit model to describe it. In Secs. V, VI, and VII, we discuss the three parameters R_0, I_s, and I_r, respectively, and develop a number of analytic results that help to provide an intuitive understanding of noise-affected I-V curves in small junctions.

II. RCSJ MODEL

As shown in Fig. 2(a), the RCSJ model consists of an ideal Josephson element of critical current I_0 shunted by a capacitance C and a resistance R_J and driven by a current source I. The ideal junction element is described by the Josephson equations,

$$I_J = I_0 \sin\phi \ , \tag{3}$$

$$\frac{d\phi}{dt} = \frac{2e}{\hbar} V \ , \tag{4}$$

where I_J is the current through the element. To describe the Johnson noise of the resistance R_J, we also include a current source I_n which represents white Gaussian noise with zero mean and autocorrelation,

$$\langle I_n(t_2) I_n(t_1) \rangle = \frac{2kT}{R_J} \delta(t_2 - t_1) \ , \tag{5}$$

where T is the temperature. In terms of dimensionless parameters, the equation of motion for the junction phase is

$$Q^2 \frac{d^2\phi}{dt'^2} + \frac{d\phi}{dt'} + \sin\phi = i + i_n(t') \ , \tag{6}$$

where $Q = (2eI_0 R_J^2 C/\hbar)^{1/2}$ is the quality factor of the linearized equation of motion, $i = I/I_0$ is the normalized dc bias, $i_n = I_n/I_0$ is the normalized noise current, and $t' = (2eI_0 R_J/\hbar)t$ is the normalized time. In this notation, $d\phi/dt' = v$ is the junction voltage V normalized to $I_0 R_J$ and the autocorrelation of i_n is

$$\langle i_n(t_2') i_n(t_1') \rangle = 2\Gamma \delta(t_2' - t_1') \ , \tag{7}$$

where $\Gamma = kT/E_J$ is the normalized temperature. The usual McCumber parameter β_c is Q^2 in our notation.

Noise-affected I-V curves computed at four normalized temperatures are shown in Fig. 6 for a RCSJ model with $Q = 5$. Each of these curves illustrates a qualitatively different situation. In the absence of noise, $\Gamma = 0$, the zero-voltage state or 0 state is stable at all bias levels less than the ideal critical current ($|i| < 1$) and the voltage state or 1 state is stable at all bias levels greater than a minimum value designated i_{r0}. For $\Gamma = 0.01$, the bias i_s at which the junction switches from the 0 state to the 1 state is suppressed below the ideal critical current and the bias i_r at which the junction returns to the 0 state is raised above i_{r0}. At a higher temperature, $\Gamma = 0.1$, the hysteresis apparent in Figs. 6(a) and 6(b) is eliminated and the I-V curve simply shows a plateau near a bias level designated i_e. In this case, the curve follows the zero-voltage axis at low bias levels but bends away from this axis as the bias approaches i_e. Finally, for $\Gamma = 1$, the I-V curve shows a finite slope at the origin indicative of phase diffusion.

The four I-V curves presented in Fig. 6 are sufficiently different that the analytic results for each case depend on a different set of assumptions. We begin by considering how the dynamics of the noise-free system determines Fig. 6(a). As noted in the Introduction, the equation of motion for the phase in the RCSJ model, Eq. (6), is equivalent to that of a damped particle in a washboard potential. Normalized to the Josephson coupling energy E_J, this potential is

$$u(\phi) = -(\cos\phi + i\phi) \ , \tag{8}$$

which is plotted for $i = 0.1$ in Fig. 7. For $|i| < 1$, the potential includes local minima and maxima at the points,

$$\phi_{\min} = \sin^{-1} i \pmod{2\pi} \ , \tag{9}$$

$$\phi_{\max} = \pi - \sin^{-1} i \pmod{2\pi} \ . \tag{10}$$

The 0 state corresponds to the particle resting at a potential minimum and is stable at bias levels ($|i| < 1$) for which such minima exist. The 1 state corresponds to the particle running down the washboard potential and is stable at bias levels ($|i| > i_{r0}$) for which the tilt of the washboard is sufficient to offset damping losses.

The return current i_{r0} at zero temperature is a parameter central to understanding the coexistence of hysteresis and phase diffusion. In the RCSJ model, i_{r0} is determined entirely by the quality factor Q and decreases with increasing Q because a smaller tilt is sufficient to support the running state when the damping is less. An accurate numerical evaluation of i_{r0} as a function of Q is shown in Fig. 8. For $Q < 0.8382$, the damping is sufficient that a running state is not possible unless the potential decreases monotonically and in this case i_{r0} is identically 1. For $Q > 0.8382$, a running state is possible even when the potential has local minima. In this case $i_{r0} < 1$ and the I-V curve is hysteretic. In the limit of large Q, Stewart[7] has shown that

$$i_{r0} = \frac{4}{\pi Q} \quad (Q \gg 1) \ , \tag{11}$$

and this approximate form for i_{r0} is plotted as a dashed line in Fig. 8. As this figure shows, Eq. (11) gives an excellent estimate of i_{r0} for Q greater than about 3 and it will be used frequently in later discussions.

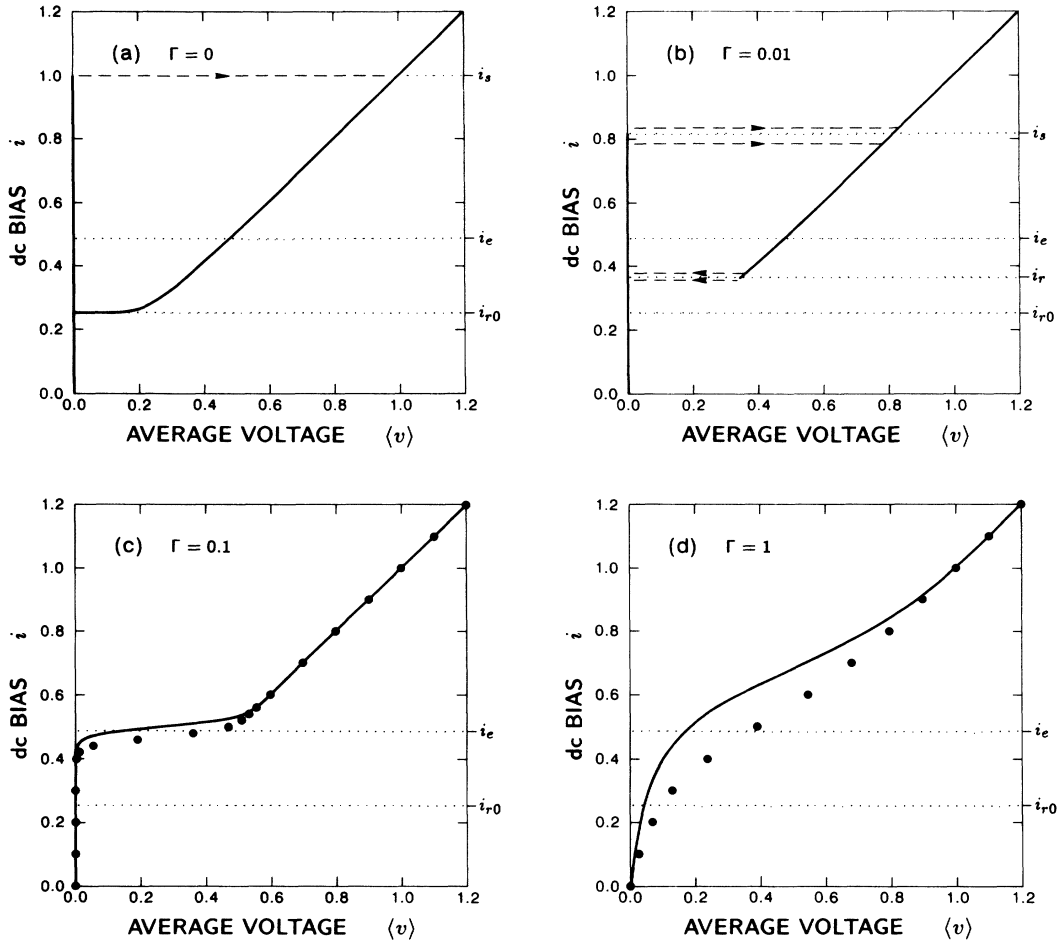

FIG. 6. Noise-affected *I-V* curves for the RCSJ model with $Q=5$ at four reduced temperatures: (a) $\Gamma=0$, (b) $\Gamma=0.01$, (c) $\Gamma=0.1$, and (d) $\Gamma=1$. The sweep rate of the dc bias is assumed to be $\alpha=10^{-10}$.

A second critical bias parameter i_m is defined as the minimum tilt at which a particle initiated at a given potential maximum with infinitesimal velocity $[\phi(0)=\phi_{\max}$ and $v(0)=\epsilon]$ will reach the next potential maximum, at $\phi_{\max}+2\pi$. This bias level is significant because the initial state it considers occurs in the process of noise-induced

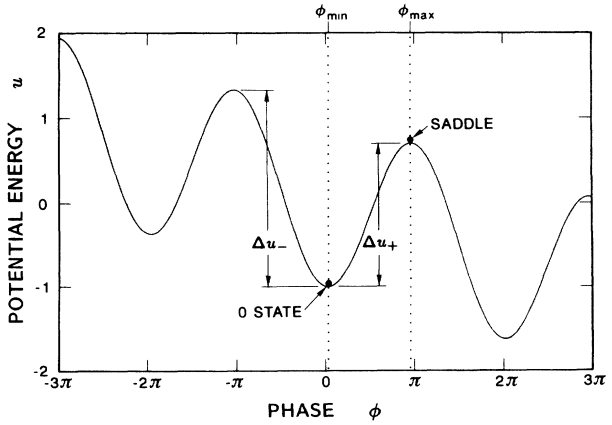

FIG. 7. Potential energy as a function of phase for the washboard analog of the RCSJ model with $i=0.1$.

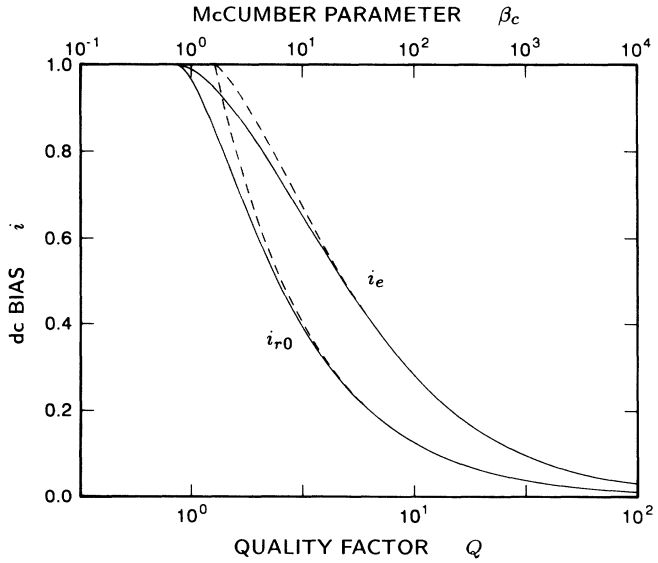

FIG. 8. Zero-temperature return current i_{r0} and equal-activation current i_e as a function of the quality factor Q. Solid lines show accurate numerical evaluations and dashed lines show approximations valid for $Q\gg1$, Eq. (11) for i_{r0} and Eq. (19) for i_e.

escape from a potential minimum in the limit of low temperature. That is, if the thermal energy available for producing escape is small, then the particle is unlikely to reach the point of escape with significant extra energy. In this case, the final result of escape will depend on whether the bias is greater or less than i_m. If $|i|<i_m$ then the particle will fail to reach the next maximum (unless it happens to get a boost from the noise source) and will be retrapped. On the other hand, if $|i|>i_m$, then the particle will clear the next potential maximum (unless it happens to be retarded by the noise source) and begin to accelerate toward the 1 state. Because a stable phase-diffusion state requires repeated escape and retrapping without switching to the 1 state, phase diffusion is possible in the low-temperature limit only at bias levels less than i_m. (We assume that noise-induced retrapping is unlikely for $|i|>i_m$ in the low-temperature limit.)

Although the parameters i_{r0} and i_m are independently defined, they are identically equal within the RCSJ model. This equality is related to the fact, noted by Belykh, Pedersen, and Soerensen,[15] that the quasiparticle branch of the I-V curve extends to zero voltage as shown in Fig. 6(a). The limiting motion associated with this branch at $i=i_{r0}$ corresponds to a particle beginning with zero velocity at a potential maximum and ending with zero velocity at the next maximum, a motion that requires infinite time and thus represents zero voltage. Because this is the same as motion that defines i_m, we conclude that $i_m=i_{r0}$. As a consequence of this equality, there is no possibility of an I-V curve with a phase-diffusion branch overlapping the quasiparticle branch in the low-temperature limit of the RCSJ model. That is, because the quasiparticle branch is stable only for $|i|>i_{r0}$ and phase diffusion in the limit of low temperature is possible only for $|i|<i_m$, there can be no hysteresis of $i_m=i_{r0}$. In Sec. III we will show that if the damping is frequency dependent then i_m can be greater than i_{r0}, allowing the phase-diffusion and quasiparticle branches to overlap.

The finite-temperature I-V curves shown in frames (b), (c), and (d) of Fig. 6 can be understood largely in terms of noise-induced transitions between the 0 and 1 states of the noise-free system. A useful perspective on such transitions is gained by examining the 0-state and 1-state attractors and their basins of attraction in state space. The typical situation for $|i|<i_{r0}$, where there is no 1-state attractor, is illustrated in Fig. 9(a) for the case $Q=5$ and $i=0.1$. Here, the phase is plotted over three oscillations of the washboard potential and the figure includes three 0-state attractors at successive potential minima. By definition, the basin of attraction of a given attractor is the region of state space that includes all sets of initial conditions leading to motion on the attractor. In the present instance, the basin boundaries coincide with the inset trajectories of the saddle points at $(\phi,v)=(\phi_{\max},0)$ and are easily calculated. The basin of the 0-state attractor near the center of Fig. 9(a) is indicated by cross hatching. If the system is initially within this central basin, a thermally induced escape can take the system to an adjacent minimum either in the $+\phi$ or $-\phi$ direction. The mean times τ'_+ and τ'_- required for such escape events, calculated within the theory of Kramers[16] and normalized to $\hbar/2eI_0R_J$, are[9,11,13,14]

$$\tau'_{\pm}=\begin{cases}\dfrac{4\pi Q^2}{\sqrt{4\mu+1}-1}\exp(\Delta u_{\pm}/\Gamma), & \Gamma<2\pi\Delta u_{\pm}/\sqrt{\mu} \quad (12a)\\ \dfrac{Q^2\Gamma}{\Delta u_{\pm}}\exp(\Delta u_{\pm}/\Gamma), & \Gamma>2\pi\Delta u_{\pm}/\sqrt{\mu}\ , \quad (12b)\end{cases}$$

where $\mu=Q^2(1-i^2)^{1/2}$ and Δu_+ and Δu_- are the potential barriers for escape in the $+\phi$ and $-\phi$ directions normalized to the Josephson coupling energy (cf. Fig. 7),

$$\Delta u_{\pm}=2(1-i^2)^{1/2}+2i(\sin^{-1}i\mp\pi/2)\ . \quad (13)$$

Although Eq. (12) is strictly valid only in the limit of low temperature ($\Gamma\ll\Delta u_{\pm}$), it also provides a useful reference point at the higher temperatures of interest here.

For $i_{r0}<|i|<1$, the 0-state and 1-state attractors coexist, and the topology of state space takes the form illustrated in Fig. 9(b) for $Q=5$ and $i=0.5$. The attractor of the 1 state is the oscillatory trajectory near $v=0.5$, and its basin of attraction is the region indicated by stippling. Because this stippled region separates the basins of adjacent 0-state attractors, it is not possible for an escape event to take the system directly from the basin of one potential minimum to that of a neighboring minimum. Instead, escape from the 0 state necessarily takes the system into the basin of the 1 state. For $i_{r0}<i<1$ (positive bias), τ'_+ is the mean time required for thermal noise to cause a transition from the basin of the 0 state to that of the 1 state. The mean time for the inverse process (transitions from the 1 state to the 0 state), although equally important to understanding noise-affected I-V curves, cannot be treated within the theory of Kramers. Thermally induced escape from the 1 state is a difficult theoretical problem because the 1 state is a dynamic nonequilibrium state. Recently, however, a number of authors have developed expressions for the mean time for escape from the 1 state using techniques suitable for nonequilibrium systems.[17–20] In particular, Ben-Jacob *et al.*[18] have obtained an analytic form for the escape time (normalized to $\hbar/2eI_0R_J$),

$$\tau'_1=Q^2\sqrt{\pi\Gamma/\Delta w}\exp(\Delta w/\Gamma)\ , \quad (14)$$

where the activation energy normalized to the Josephson coupling energy is given approximately by

$$\Delta w=\tfrac{1}{2}Q^2(i-i_{r0})^2\ . \quad (15)$$

Equations (14) and (15) are valid in the limit of low temperature ($\Gamma\ll\Delta w$) and low damping $Q\gg1$. Because the process of escape from the 1 state is one in which the noise source acts as a brake to stop the motion of the particle down the washboard, it is not surprising that the activation energy Δw is approximately equal to $\frac{1}{2}Q^2\langle d\phi/dt'\rangle^2$, the average kinetic energy of the particle in the 1 state.

Equations (12) and (14) for $\tau'_{\pm}$ and τ'_1 provide all of the information necessary for understanding noise-affected I-V curves in the low-temperature limit. In this limit, the

mean escape times are dominated by the exponential factors $\exp(\Delta u_{\pm}/\Gamma)$ and $\exp(\Delta w/\Gamma)$ which can change by many orders of magnitude with small changes in the activation energies $\Delta u_{\pm}$ and Δw. These activation energies are plotted in Fig. 10 as a function of dc bias for $Q=5$. While the expression for $\Delta u_{\pm}$ given by Eq. (13) is exact, that for Δw given by Eq. (15) is only approximate. Recently, a number of authors[21–24] have developed techniques for the accurate numerical evaluation of Δw, and Fig. 10 compares the accurate Δw (solid line) with the analytic approximation (dashed line). Over bias regions for which the activation energies are much greater than Γ, the exponential factors of Eqs. (12) and (14) can be large enough that the mean time for escape greatly exceeds the duration of a typical experiment even though the prefactors of the exponentials represent relatively short times, on the order of either $R_J C$ or $1/\omega_p$. In these bias regions the 0 and 1 states are stable despite the presence of noise. On the other hand, Δu_+ goes to 0 as i approaches 1 from below and Δw goes to 0 as i approaches i_{r0} from above. In these bias regions, the exponential factors approach 1 and the escape times are on the order of $R_J C$ or $1/w_p$, which are typically much shorter than measurement times. Thus, noise can dramatically reduce the stability of the 0 state just below the critical current and the stability of the 1 state just above the zero-temperature return current.

Consider now the I-V curve for $\Gamma=0.01$ shown in Fig. 6(b). To be quantitative about escape times, we will assume that $I_0 R_J=2$ mV, so $\hbar/2eI_0R_J=0.165$ ps. At $i=0$, the exponential factor determining $\tau_{\pm}=(\hbar/2\epsilon I_0 R_J)\tau'_{\pm}$ is $\exp(200)$ and the prefactor is 5.7

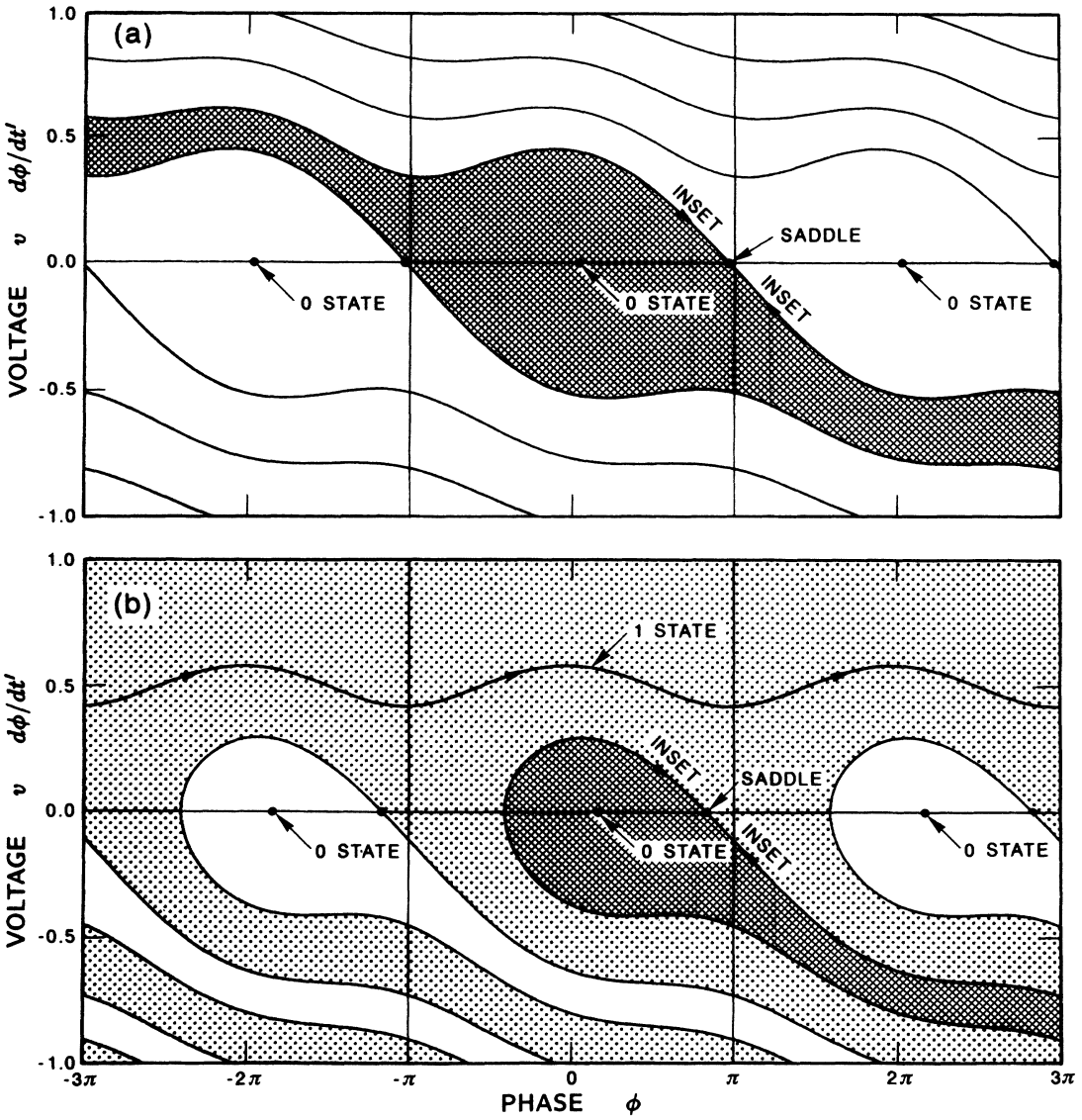

FIG. 9. State-space diagrams of the RCSJ model showing the attractors and their basins of attraction for $Q=5$ with (a) $i=0.1$ and (b) $i=0.5$. The basin of attraction of the 1 state is stippled and those of the 0 states are either clear or crosshatched.

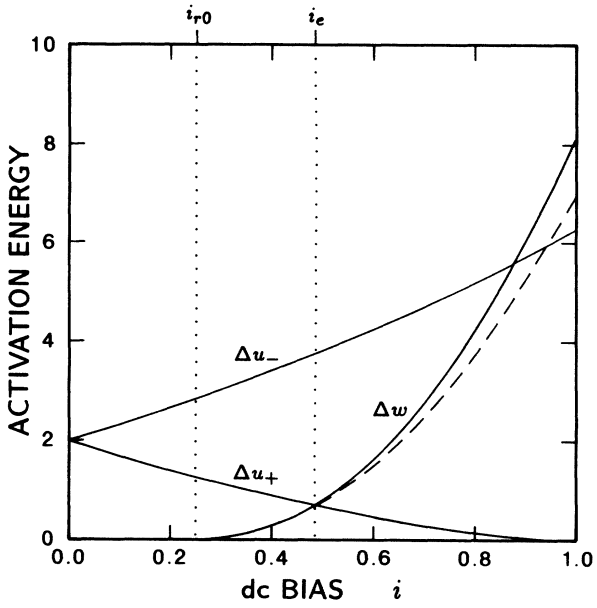

FIG. 10. Activation energies for escape from the 0-state and 1-state attractors as a function of dc bias for $Q=5$. Accurate numerical results for Δw are shown as a solid line (Ref. 23) and the approximate expression given by Eq. (15) is plotted as a dashed line. Energies are normalized to the Josephson coupling energy E_J.

ps, so the mean time for escape from a potential minimum is 4.1×10^{75} s. Because this time exceeds the age of the universe, the 0 state at $i=0$ is completely stable for practical purposes. However, as the dc bias is increased to trace the *I-V* curve, τ_+ decreases rapidly due to the decrease in Δu_+ and drops below 1 s as the bias reaches $i=0.74$. Thus, at bias levels approaching the critical current, thermal noise makes the 0 state highly unstable and the junction is likely to switch to the 1 state. The statistics of this switching process have been examined in detail both theoretically[11,25–27] and experimentally.[12,28–35] Assuming that the dc bias increases from $i=0$ at a rate $\alpha=|di/dt'|$, the probability $P_0(i)$ that the junction remains in the 0 state when the bias level reaches i is[26]

$$P_0(i)=\exp\left[-\int_0^i di'\frac{1}{\alpha\tau'_+(i')}\right]. \tag{16}$$

In the *I-V* curve of Fig. 6(b), we assume that $\alpha=10^{-10}$, such that the bias is swept from 0 to the critical current in 1.65 ms. For this sweep rate, the probability of remaining in the 0 state is 0.99 at $i=0.785$ and 0.01 at $i=0.834$, so that 98% of all switching events occur between these two bias levels [shown as dashed lines in Fig. 6(b)]. Thus, although the switching current varies with each sweep of the dc bias, the range of switch points is sufficiently narrow that it is useful to define the switching current i_s as the bias at which $P_0=0.5$. In Fig. 6(b), $i_s=0.817$.

Because the lifetime of the 1 state at $i=i_s$ in Fig. 6(b), is, according to Eq. (14), 6.3×10^{160} s, there is no chance that the junction will switch back to the 0 state after an escape event. However, when the bias is decreased, the stability time of the 1 state falls rapidly and a return to the 0 state becomes probable as i approaches $i_{r0}=0.252$. Given that the junction begins in the 1 state at $i=1$ and the bias is decreased at a rate α, the probability $P_1(i)$ that the junction remains in the 1 state when the bias reaches i is

$$P_1(i)=\exp\left[-\int_i^1 di'\frac{1}{\alpha\tau'_1(i')}\right]. \tag{17}$$

In the case of return from the 1 state, Eq. (17) shows that 98% of the switching events occur between $i=0.377$ and $i=0.356$, a range of bias indicated by dashed lines in Fig. 6(b). If we define the return current to be the bias at which $P_1=0.5$, then $i_r=0.363$ in the present case. We conclude that at $\Gamma=0.01$, the *I-V* curve is similar to the hysteretic characteristic of the noise-free junction but there is a reduction in overlap between the two stable branches due to premature switching events induced by thermal noise.

A question of particular importance in the present paper concerns the voltage of the 0 state at bias points near i_s in Fig. 6(b). Does the junction always switch to the 1 state after escaping from a potential minimum or is there a significant probability of retrapping in a nearby well before the transition to the 1 state is complete? This question was recently answered by Silvestrini and Cristiano[36] who show that in the limit of low damping ($Q\gg1$) and low temperature ($\Gamma\ll1$), the probability of retrapping at bias levels well above i_{r0} is much less than 1. That is, almost all escape events at bias levels near i_s lead directly to the 1 state, and phase diffusion, which requires repeated escape and retrapping events, is not possible. Thus, no significant voltage is associated with the 0-state branch in Fig. 6(b).

At temperatures above $\Gamma=0.01$, the overlap between the 0-state and 1-state branches is reduced from that shown in Fig. 6(b) and, at sufficiently high temperatures, the *I-V* curve is nonhysteretic. This situation is shown in Fig. 6(c) for $\Gamma=0.1$. When the parameters i_s and i_r are calculated at $\Gamma=0.1$ based on the conditions $P_0(i_s)=0.5$ and $P_1(i_r)=0.5$, we find $i_s=0.301$ and $i_r=0.615$. Thus, both the 0 state and the 1 state are unstable in the bias range $0.301<i<0.615$, resulting in a situation where the junction switches rapidly back and forth between these two states. *I-V* curves for this situation have been calculated both analytically[17] and through Monte Carlo simulations,[37,38] and both approaches are illustrated in Fig. 6(c). The analytic result for the voltage, shown by a solid line, is calculated as the average of the voltages of the noise-free 0 and 1 states weighted by the time the junction spends in each state. That is,

$$\langle v\rangle=\frac{\tau'_1}{\tau'_+ +\tau'_1}v_1, \tag{18}$$

where v_1 is the voltage of the 1 state in the absence of

noise. The Monte Carlo results, shown by solid circles, were obtained by integrating the equation of motion, Eq. (6), and computing the average voltage over a normalized time of 10^7 units (1.65 μs). In this calculation, the noise current i_n was represented by a Gaussian random number generator with a mean of 0 and a variance of $\langle i_n^2 \rangle = 2\Gamma/\Delta t'$, where $\Delta t'$ is the time step used in the integration. Because the integration routine passed extensive tests in earlier work,[23] the small discrepancy between the two curves plotted in Fig. 6(c) can probably be attributed to the approximations involved in the analytic result [Eqs. (12), (14), and (18)].

The I-V curve of Fig. 6(c) shows a rapid transition near $i=0.5$ from voltages near 0 to voltages near that of the noise-free 1 state. According to Eq. (18), the midpoint of this transition occurs at the bias level where $\tau'_+ = \tau'_1$ and the junction spends equal time in the 0 and 1 states. Although this bias level is in principle temperature dependent, the dependence is sufficiently weak that its low-temperature limit i_e provides a good approximation to the transition level at all temperatures. Because the exponential factors in Eqs. (12) and (14) dominate the expressions for τ'_+ and τ'_1 in the limit of low temperature, i_e is simply the bias at which $\Delta u_+ = \Delta w$ (cf. Fig. 10). Defined in this way, as the bias at which the stability energies of the 0 and 1 states are equal, i_e is a function only of the quality factor Q. This parameter is plotted as a function of Q in Fig. 8, where a solid line shows an accurate result for i_e based on the numerical evaluation[23] of Δw and a dashed line shows an approximate result,

$$2(1-i_e^2)^{1/2} + 2i_e(\sin^{-1} i_e - \pi/2) = \tfrac{1}{2}Q^2(i_e - i_{r0})^2 , \qquad (19)$$

based on Eq. (15). As Fig. 8 shows, the agreement between Eq. (19) and the accurate result is excellent for values of Q above about 3. Although Eq. (19) cannot be solved explicitly for i_e, it has the approximate solution,

$$i_e = (2+4/\pi)Q^{-1} + (2+\pi)Q^{-2} , \qquad (20)$$

in the limit of large Q. This form for i_e allows a comparison with the work of Vollmer and Risken[17] who numerically evaluated the coefficient of Q^{-1} to be 3.3576, in good agreement with our result of $2+4/\pi = 3.2732$. The bias level i_e is significant because it defines the point at which the switching currents i_s and i_r coalesce when the temperature is increased to the point where hysteresis is eliminated from the I-V curve.

With the introduction of I_e, we have defined all but one of the seven bias-current parameters that will be used in discussing noise-affected I-V characteristics. For future reference, the definitions of all seven parameters are listed in Table I.

In formulating Eq. (18) for the average voltage, we have postulated that the junction switches rapidly between the 0 and 1 states at bias levels near i_e. This behavior is verified by our Monte Carlo simulations. In Fig. 11(a) we plot the junction voltage as a function of time for a bias point, $i=0.47$, near the center of the transition region. The waveform of Fig. 11(a) approximates a random telegraph signal with switching at irregular intervals between two distinct levels near $v=0$ and $v=v_1$. Thus, in contrast with the phase-diffusion process shown in Fig. 5 where the voltage of the running state remains well below the voltage of the quasiparticle branch, we find in Fig. 11(a) a process in which escape from the 0 state almost invariably leads to occupation of the 1 state for an extended period. However, the stability times of the 0 and 1 state observed here, on the order of 2×10^5 time units or 0.033 μs, are short enough that only the average voltage would be observed in a typical experimental I-V curve. The telegraphic waveform shown in Fig. 11(a) is exactly that required for the validity of Eq. (18) and explains the accuracy of this equation.

For the I-V curve shown in Fig. 6(c), the probability of an escape from the 0 state occurring as the bias is swept from 0 to i_{r0} is less than 0.001 according to Eq. (16). Thus, no significant voltage is associated with this part of the I-V curve. At higher temperatures, however, escape from the 0 state becomes probable even near $i=0$, and gives rise to an I-V curve with a finite slope at the origin, as shown in Fig. 6(d) for $\Gamma=1$. Equation (18), which predicts zero voltage at bias levels below i_{r0} where there is no 1 state, is not valid in this higher-temperature regime be-

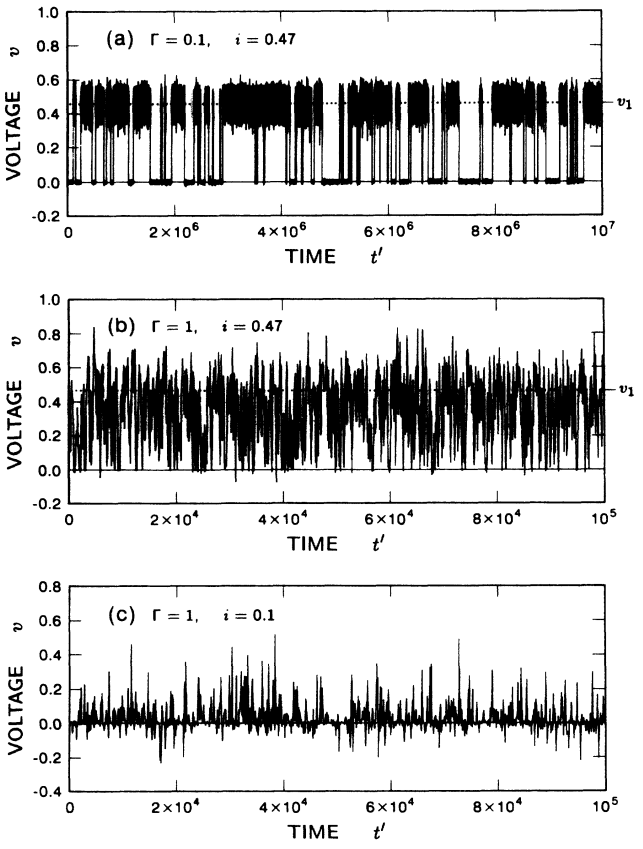

FIG. 11. Voltage as a function of time for the $Q=5$ RCSJ model with (a) $\Gamma=0.1$ and $i=0.47$, (b) $\Gamma=1$ and $i=0.47$, and (c) $\Gamma=1$ and $i=0.1$. High-frequency noise has been removed from these curves by plotting voltage averaged over 100 time units.

TABLE I. Definitions of bias-current parameters.

I_0	*Ideal critical current*: the current at which the junction switches from the zero-voltage branch of the *I-V* curve to the quasiparticle branch in the absence of noise.
I_s	*Switching current*: the current at which the junction switches from the zero-voltage or phase-diffusion branch of the *I-V* curve to the quasiparticle branch in the presence of noise.
I_r	*Return current*: the current at which the junction switches from the quasiparticle branch to the zero-voltage or phase-diffusion branch in the presence of noise.
I_{r0}	*Noise-free return current*: the current at which the junction switches from the quasiparticle branch to the zero-voltage branch in the absence of noise.
I_m	*Minimum escape current*: the minimum current for which the noise-free system switches to the 1 state when initialized at a maximum of the washboard potential with no voltage on the junction or external capacitances.
I_t	*Threshold current*: the minimum current for which the noise-free system switches to the 1 state when initialized at a maximum of the washboard potential with specified voltages on the junction and external capacitances.
I_e	*Equal-stability current*: the current at which the activation energies for escape from the 0 state and 1 state are equal.

cause it does not account for events in which the 1 state is not attained after escape from the 0 state. In Fig. 6(d) we show for $\Gamma=1$ the results of two other types of calculation: Monte Carlo simulations, indicated by solid circles, and a solution of the Fokker-Planck equation due to Vollmer and Risken,[17] indicated by a solid line. The Monte Carlo results shown here are presumed to be accurate, whereas the Fokker-Planck curve represents an asymptotic form that is strictly valid only in the limit of large Q. The discrepancy between the two calculations probably results because $Q=5$ is not large enough to apply the asymptotic form. However, both curves show the same qualitative features, including a finite slope at the origin.

The dynamical behavior of the junction at $\Gamma=1$ is illustrated in Figs. 11(b) and 11(c) for the bias levels $i=0.47$ and $i=0.1$ respectively. Comparing the voltage waveform of Fig. 11(b) for $\Gamma=1$ with that of Fig. 11(a) for $\Gamma=0.1$, we find that the random telegraph signal of low temperatures is replaced by a much less regular stochastic process at higher temperatures. This dynamical difference gives a second reason why Eq. (18) is not valid at $\Gamma=1$. At $i=0.47$ and $\Gamma=1$, the noise is simply too great to yield a well-defined telegraph signal. At $i=0.1$, on the other hand, a telegraph signal cannot be expected because a 1 state does not exist in the noise-free system for $i<i_{r0}=0.252$. Instead, we find in Fig. 11(c) a random process in which the junction spends significant time trapped in a potential well with a voltage near 0 and occasional escape events producing voltage spikes as the junction moves between wells in either the $+\phi$ or $-\phi$ direction. This phase-diffusion process, described previously in the Introduction, will be considered in detail in Sec. V.

To conclude our discussion of the RCSJ model, we return to the question of whether this model allows the coexistence of phase diffusion and hysteresis in a single *I-V* curve. That is, does there exist a set of parameters Q, Γ, and α for which repeated escape and retrapping events would give a small voltage to the nominal zero-voltage state at a bias level for which the quasiparticle branch is also stable? We argued above that this situation is not possible in the limit of zero temperature because retrapping is not possible for bias levels above i_{r0} and the quasiparticle branch does not exist for bias levels below i_{r0}. We also noted that this conclusion is extended to finite temperatures by the work of Silvestrini and Cristiano,[36] who have shown that retrapping is unlikely at bias levels well above i_{r0} in the limit of large Q. The possibility remains that retrapping is highly probable at bias levels just above i_{r0} at finite temperatures. This scenario is given plausibility by the fact that the fingers of the 1-state attractor that separate neighboring 0-state attractors [cf. Fig. 9(b)] are very narrow at bias levels near i_{r0}. At low temperatures, escape from the 0 state usually occurs near the saddle point and, in the limit of large Q, the trajectory hugs the boundary of the 0-state attractor for many oscillations of the washboard potential after escape occurs. During this initial portion of the switching process, there is a chance that thermal noise will knock the system back into one of the 0-state attractors and cause retrapping. As i approaches i_{r0} and the trajectory hugs the 0-state attractors ever more tightly, the situation becomes akin to walking along the edge of a cliff in a windstorm and the probability of reaching the 1 state approaches 0. Thus, we might argue that repeated escape and retrapping events can occur at bias levels just above i_{r0}, allowing phase diffusion at a point where the quasiparticle branch is also stable.

Although we will find the cliff-edge scenario useful in another context, it leads to an incorrect conclusion for the RCSJ model. The problem is that temperatures high enough to produce significant numbers of 0-state escape events at bias levels near i_{r0} are also high enough to de-

stabilize the 1 state in this bias range. Indeed, we have already shown that hysteresis can occur in the RCSJ model only when the temperature is sufficiently low that the 0 state is stable at all bias points below i_e. Thus, if phase diffusion and hysteresis are to coexist in the same I-V curve, the phase diffusion must take place at bias levels above i_e. Because i_e is always substantially greater than i_{r0} [cf. Fig. 8 and Eqs. (11) and (20)], the relevant state-space diagram is one in which the 0-state attractors are well separated and retrapping events are expected to be unlikely. This argument suggests that there is no combination of Q, Γ, and α for which phase diffusion and hysteresis coexist. Detailed Monte Carlo simulations carried out at both $Q=5$ and $Q=100$ also support this conclusion. We are thus led to the belief that the experimental I-V curve shown in Fig. 1 cannot be explained even qualitatively by the simple RCSJ model.

III. FREQUENCY-DEPENDENT DAMPING

Noise-affected I-V curves in which the phase-diffusion and quasiparticle branches overlap can be obtained by extending the RCSJ model to include frequency-dependent damping. Perhaps the simplest such extension consists of the RCSJ model plus a shunt composed of a resistor R_s, its associated Johnson noise source I_{n1}, and a capacitor C_b, as shown in Fig. 2(b). The additional circuit elements of this model can be used to represent an external circuit that loads the junction. For example, if the leads attached to measure the I-V curve behave as a lossy transmission line at microwave frequencies, then R_s might be chosen as the characteristic impedance of the line and C_b might be chosen to control the disappearance of this loading at lower frequencies. On the other hand, our experiment, shown in Fig. 3, is approximately modeled by choosing R_s as the parallel combination of the two isolation resistors and C_b as the capacitance of the leads. However, because this approximate model is not adequate to describe our experiment quantitatively, our primary interest in the circuit of Fig. 2(b) derives from the fact that it provides a simple system for understanding the qualitative changes introduced by frequency-dependent damping.

As in the case of the RCSJ model, it is convenient to describe the circuit of Fig. 2(b) in terms of dimensionless variables. If we define the dimensionless quantities,

$$t'=t(2eI_0R_J/\hbar)\ , \tag{21}$$

$$v=V/I_0R_J\ , \tag{22}$$

$$v_b=V_b/I_0R_J\ , \tag{23}$$

$$i=I/I_0\ , \tag{24}$$

$$i_n=I_n/I_0\ , \tag{25}$$

$$i_{n1}=I_{n1}/I_0\ , \tag{26}$$

$$Q_0=R_J\sqrt{2eI_0C/\hbar}\ , \tag{27}$$

$$Q_1=(1/R_J+1/R_s)^{-1}\sqrt{2eI_0C/\hbar}\ , \tag{28}$$

$$\rho=R_JC/R_sC_b\ , \tag{29}$$

$$\Gamma=2ekT/\hbar I_0\ , \tag{30}$$

then the equations of motion take the form,

$$\frac{d\phi}{dt'}=v\ , \tag{31}$$

$$\frac{dv}{dt'}=Q_0^{-2}[i+i_n+i_{n1}-\sin\phi+v+(v_b-v)(Q_0/Q_1-1)]\ , \tag{32}$$

$$\frac{dv_b}{dt'}=\rho Q_0^{-2}[v-v_b-i_{n1}/(Q_0/Q_1-1)]\ . \tag{33}$$

Assuming both resistors are at the same temperature, the autocorrelation functions of the noise sources are

$$\langle i_n(t_2')i_n(t_1')\rangle=2\Gamma\delta(t_2'-t_1')\ , \tag{34}$$

$$\langle i_{n1}(t_2')i_{n1}(t_1')\rangle=2\Gamma(Q_0/Q_1-1)\delta(t_2'-t_1')\ . \tag{35}$$

The dimensionless parameters introduced here are similar to those used for the RCSJ model but include in addition the voltage v_b across the external capacitance, the Johnson noise current i_{n1} of the external resistance, a second quality factor Q_1, and the ratio ρ of the R-C time of the junction to that of the external shunt. The equations of motion for the extended system are equivalent to a third-order differential equation, and three state variables, ϕ, v, and v_b, are required to describe the dynamics. The normalized I-V characteristic is determined by the three parameters Q_0, Q_1, and ρ in the absence of noise and, at finite temperatures, the two additional parameters Γ and $\alpha=|di/dt'|$ are required.

As our primary example, we consider the case $Q_0=5$, $Q_1=2$, and $\rho=0.1$, which corresponds to the RCSJ example considered in the Sec. III modified by the addition of a shunt that increases the damping at high frequencies. In order to quantify the damping introduced by this modification, we define a frequency-dependent quality factor,

$$Q(\omega)=[2eI_0C/\hbar G^2(\omega)]^{1/2}\ , \tag{36}$$

where

$$G(\omega)=\frac{1+(R_J/R_\parallel)R_s^2C_b^2\omega^2}{R_J(1+R_s^2C_b^2\omega^2)} \tag{37}$$

is the real part of the admittance shunting the ideal Josephson element. Here $R_\parallel=(R_J^{-1}+R_s^{-1})^{-1}$ is the parallel combination of R_J and R_s. In terms of dimensionless parameters, the quality factor can be written as

$$Q(\omega)=Q_0\frac{1+Q_0^2\rho^{-2}(\omega/\omega_p)^2}{1+Q_0^3Q_1^{-1}\rho^{-2}(\omega/\omega_p)^2}\ , \tag{38}$$

where $\omega_p=\sqrt{2eI_0/\hbar C}$ is again the plasma frequency. (For the cases of interest here, the plasma resonance is shifted only slightly from ω_p by the capacitance C_b.) The quality factor is plotted as a function of frequency in Fig. 12 for our example. At low frequencies, the quality factor is approximately $Q_0=5$ because C_b is an effective open circuit and the damping is determined by R_J alone. At high frequencies, C_b is an effective short, the damping

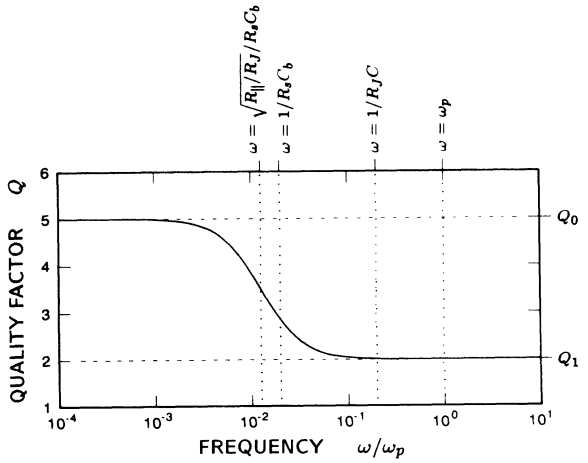

FIG. 12. Quality factor as a function of frequency for the circuit model of Fig. 2(b) as given by Eq. (38) with $Q_0=5$, $Q_1=2$, and $\rho=0.1$.

is determined by the parallel combination of R_J and R_s, and Q is approximately $Q_1=2$. The transition between these low- and high-damping regimes occurs near $\omega=1/R_sC_b$. By choosing $\rho=0.1$, we have placed this transition frequency a factor of 10 below the junction's $1/R_JC$ frequency which is itself a factor of Q_0 below the plasma frequency. Thus, in our example, the damping at the plasma frequency is much greater than at low frequencies, creating the type of situation in which we expect to find phase diffusion in a hysteretic I-V curve.

Noise-affected I-V curves calculated through Monte Carlo simulations for the case $Q_0=5$, $Q_1=2$, and $\rho=0.1$ are shown in Fig. 13 for four temperatures. In this figure, the time over which a solution must persist to be considered stable is defined by the time (10^7 units) that the bias is required to dwell at a given level rather than by the slew rate α. The I-V curve for $\Gamma=0$ shown in Fig. 13(a) is qualitatively similar to that for the noise-free RCSJ model [Fig. 6(a)] except in one respect: in the case of frequency-dependent damping, the 1 state does not extend to zero voltage as it does in the RCSJ model. As we discuss below, this difference is crucial to the existence of phase diffusion in hysteretic I-V curves. Just such hysteretic I-V curves are illustrated in Figs. 13(b) and 13(c) for $\Gamma=0.08$ and $\Gamma=0.1$. These figures show I-V curves that are, at first glance, similar to the RCSJ characteristic of Fig. 6(b) but with smaller regions of hysteresis. However, when the nominal zero-voltage branches of Figs.

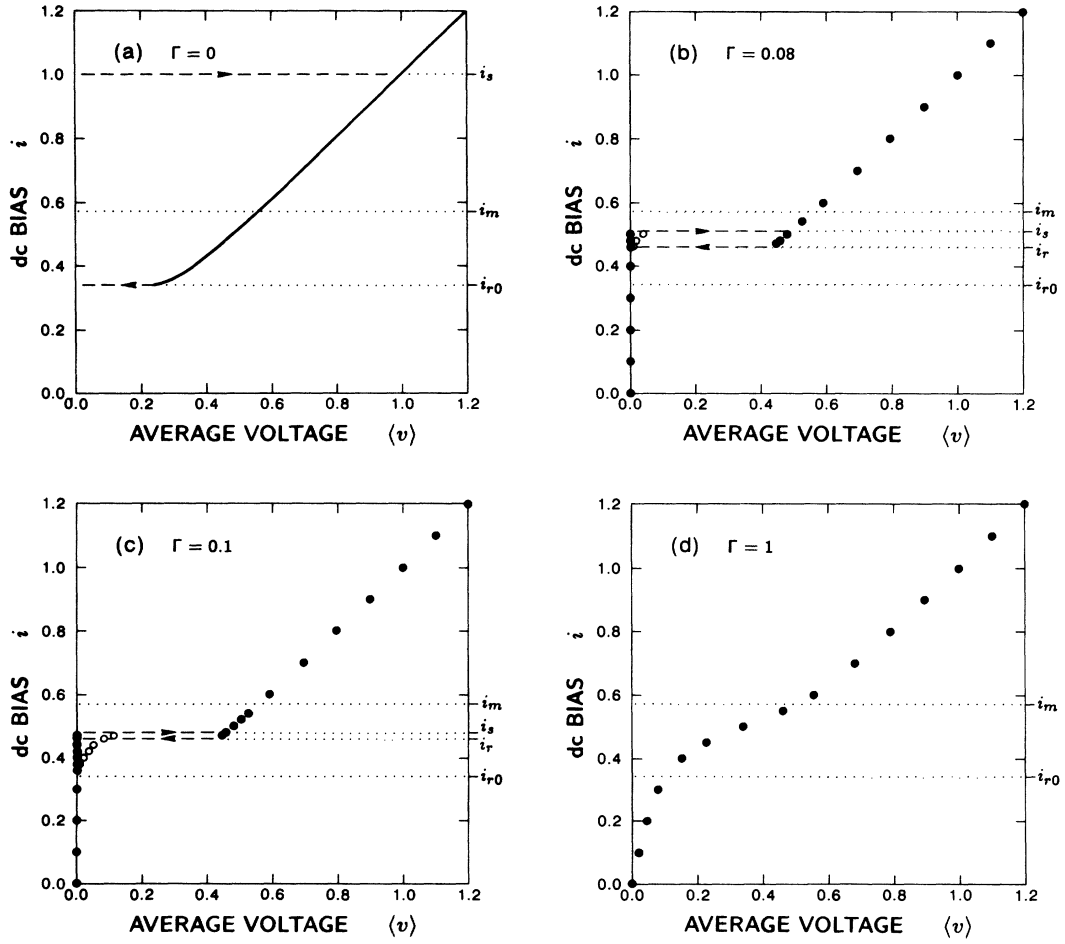

FIG. 13. Noise-affected I-V curves for the circuit model of Fig. 2(b) with $Q_0=5$, $Q_1=2$, and $\rho=0.1$ at temperatures of (a) $\Gamma=0$, (b) $\Gamma=0.08$, (c) $\Gamma=0.1$, and (d) $\Gamma=1$. In frames (b), (c), and (d), voltages were calculated through Monte Carlo simulations using an averaging time of 10^7 units. The open circles in frames (b) and (c) show the voltage of the phase-diffusion state multiplied by a factor of 1000.

13(b) and 13(c) are examined closely, the voltage is found to be nonzero at bias levels near the switching current i_s. Open circles show this voltage magnified by a factor of 1000. Thus, as anticipated, Figs. 13(b) and 13(c) show a phase-diffusion branch that overlaps the quasiparticle branch. They do not, however, evidence a finite slope at the origin, one of the characteristics of the experimental I-V curves that we hope to explain. For the chosen parameter set, such a slope develops only at higher temperatures where the I-V curve is not hysteretic, as illustrated in Fig. 13(d) for $\Gamma=1$. At the end of this section we consider a parameter set with reduced damping for which the phase-diffusion branch has a finite slope at the origin and also overlaps the quasiparticle branch. First, however, we focus on understanding the I-V curves shown in Fig. 13, beginning with the noise-free system.

For the system of Fig. 2(b), we define the parameter i_m to be the minimum bias for which the noise-free system will reach $\phi=\phi_{\max}+2\pi$, if it is initiated at $\phi=\phi_{\max}$ with an infinitesimal junction voltage ($v=\epsilon$) and no voltage on the external capacitor ($v_b=0$). As with the RCSJ model, i_m defines the bias below which phase diffusion can occur in the limit of low temperatures. That is, if escape from the 0 state occurs with no extra energy, then the system will switch to the 1 state if $|i|>i_m$ but return to the 0 state if $|i|<i_m$. Because the quasiparticle branch does not extend to zero voltage in Fig. 13(a) we cannot argue that i_m is equal to the zero-temperature return current i_{r0} as in the RCSJ model. Numerical evaluation of these two parameters yields $i_m=0.572$ and $i_{r0}=0.343$ for the case considered in Fig. 13. The fact that i_m exceeds i_{r0} is important because it implies a bias range $i_{r0}<|i|<i_m$ where a phase-diffusion branch can overlap the quasiparticle branch, at least in the limit of low temperature.

The relative values of i_m and i_{r0} in the case of frequency-dependent damping can be understood qualitatively by extending the formula $i_m=i_{r0}=4/\pi Q$ for the RCSJ model. Because the motion that defines i_m is essentially a half cycle of the plasma oscillation, the relevant quality factor is $Q(\omega_p)\equiv Q_p\approx Q_1$ and we might suppose that

$$i_m\approx\frac{4}{\pi Q_p}\approx\frac{4}{\pi Q_1}\ . \tag{39}$$

In contrast, the dynamics of a junction biased at finite voltages on the quasiparticle branch corresponds to a roughly steady motion down the washboard potential, suggesting that $Q(0)=Q_0$ is the quality factor relevant to the return process and that

$$i_{r0}\approx\frac{4}{\pi Q_0}\ . \tag{40}$$

Although these expressions for i_m and i_{r0} are not especially accurate in the present instance (they yield $i_m=0.637$ and $i_{r0}=0.255$), the expression for i_m is accurate in the limit of large Q_1, as we verify later in this section, and the expression for i_{r0} roughly approximates a form derived in Sec. VII, where we show that i_{r0} is only weakly dependent on the damping at high frequencies. Given the basic validity of Eqs. (39) and (40), we conclude that i_m is greater than i_{r0} for the model of Fig. 2(b) because the damping is greater at the plasma frequency than at low frequencies.

The consequences of the relation $i_m>i_{r0}$ are illustrated most clearly by the topology of the basins of attraction in state space. Although the state space is three dimensional in the case of frequency-dependent damping, the basins of attraction are similar to those of the RCSJ model for both $|i|<i_{r0}$ and $|i|>i_m$. That is, for $|i|<i_{r0}$, the only attractors are the fixed points at potential minima, and the basins of attraction of adjacent minima are contiguous as in Fig. 9(a). Similarly, for $|i|>i_m$, the basins of attraction are like those of Fig. 9(b), with fingers of the 1-state basin separating the 0-state basins. However, for $i_{r0}<|i|<i_m$, the basins of attraction are topologically different from those of the RCSJ model. The basins for a bias point, $i=0.5$, in this range are illustrated in Fig. 14 where we show a cross section of state space defined by the $v_b=0$ plane. This cross section includes both the 0-state attractors and the saddle points but does not intersect the 1-state attractor, for which v_b is everywhere nonzero. Figure 14 does, however, include part of the 1-state basin, indicated by stippling. The important topological feature of Fig. 14 is the fact that the basins of adjacent 0-state attractors are contiguous even though there is a coexisting 1-state attractor. Thus, for bias levels in the range $i_{r0}<|i|<i_m$, thermal noise can produce transitions between potential minima in which the state-space trajectory does not enter the basin of the 1 state. This topology opens the possibility of repeated noise-induced events in which the system escapes from a potential minimum and retraps in a nearby minimum without a significant probability of switching to the 1 state.

For the situation shown in Fig. 14, a given 0-state attractor is contiguous to its two neighboring 0-state attractors and to the 1-state attractor. In this case, we can define four different lifetimes: the mean times $\tau_\pm$ for escape from the basin of a given potential minimum in the $+\phi$ and $-\phi$ directions, the mean time τ_0 for escape from the collective basin of the 0-state attractors to the basin of the 1 state, and the mean time τ_1 for escape from the 1-state basin to the collective 0-state basin. To obtain phase diffusion in a hysteretic I-V curve we must have $\tau_\pm\ll\tau_0$ and $\tau_\pm\ll\tau_1$, such that transitions between potential minima are much more probable than transitions in either direction between the 1 state and the 0 state. This condition allows overlap between a phase-diffusion branch and the quasiparticle branch of the I-V curve.

The dynamics of noise-induced transitions between basins of attraction having the topology of Fig. 14 are illustrated in Fig. 15. This figure shows typical transitions for selected points on the I-V curve of Fig. 13(c) where there is a small overlap between the phase-diffusion and quasiparticle branches. At $i=0.47$, both branches are stable on a time scale of 10^7 units, the time the bias is assumed to dwell at a given value, and transitions between branches were not observed. However, when biased on the phase-diffusion branch, noise-induced transitions between potential minima occur roughly once in 10^5 time units. An event of this type is shown in Fig. 15(a) where we plot both the junction voltage v and the voltage across

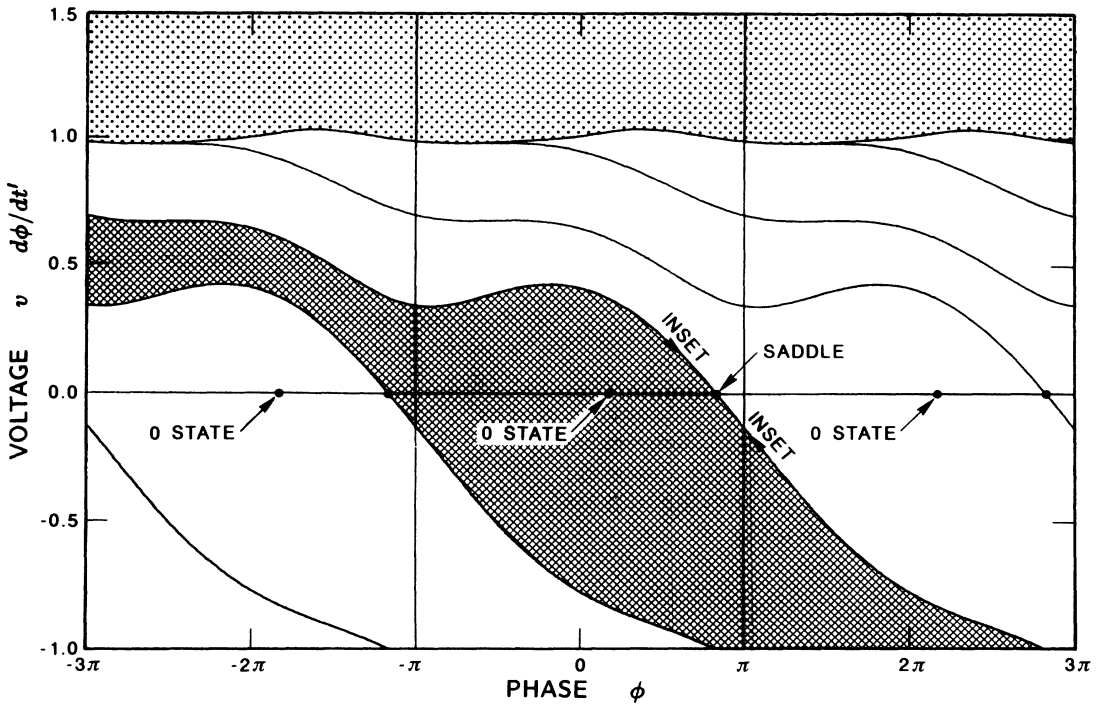

FIG. 14. State-space diagram for the model of Fig. 2(b) with $Q_0=5$, $Q_1=2$, $\rho=0.1$, and $i=0.5$. A cross section is shown through the plane $v_b=0$. The basin of the central 0-state attractor is crosshatched and that of the 1-state attractor is stippled.

the external capacitance v_b. During most of the time interval shown, the junction executes noise-induced plasma oscillations about a potential minimum but, near $t'=1000$, noise causes escape from the minimum initially occupied, followed by retrapping in a minimum displaced down the washboard by $\Delta\phi=4\pi$. During this phase-slip event, the junction voltage approaches v_1, the average voltage of the quasiparticle branch, but the voltage on the external capacitance is not significantly affected due to the long time constant for charging C_b. Even though v approaches v_1, the system remains within the collective basin of the 0-state attractors during the phase-slip process. This can be seen from Fig. 14, which shows that the collective 0-state basin extends almost to $v=1$ when v_b is near 0. Thus, at $i=0.47$, phase slips can occur without crossing the 1-state basin, and the probability of switching to the quasiparticle branch is small even though the frequency of phase slips is high ($\tau_+ \ll \tau_0$).

At $i=0.48$ in Fig. 13(c), τ_0 is approximately 10^7 time units, and switching from the phase-diffusion branch to the quasiparticle branch is probable during the assumed dwell time. A switching event of this type is shown in Fig. 15(b). The switching process begins with noise-induced escape from a potential minimum, but additional noise prevents the junction from retrapping in a nearby minimum, and the process continues as the external capacitance is slowly charged to the average voltage of the quasiparticle branch. When the switch is complete, the voltage oscillations are at the Josephson frequency $\omega_J=2eV_1/\hbar$. For $\rho \ll 1$, the time constant for charging C_b is approximately $(R_J+R_s)C_b$ or $Q_0^3/\rho Q_1=625$ in normalized time, assuming the junction is an open circuit. Because the charging time is relatively long, the junction has many opportunities to retrap in a potential minimum before the switch to the voltage state is complete, and, indeed, retrapping occurs much more frequently than the switching event shown in Fig. 15(b). Thus, the fact that $\tau_+ \ll \tau_0$, as required to observe phase diffusion in a hysteretic junction, results in part from the long time required to charge the external capacitor. At $i=0.48$, however, τ_0 is itself as short as the dwell time, and switching to the quasiparticle branch is probable.

The reverse switching process is illustrated at the bias point $i=0.46$ in Fig. 13(c), where τ_1 is approximately 10^7 time units and switching from the 1 state to the 0 state is probable during the dwell time. A switching event of this type is shown in Fig. 15(c). Here the junction voltage switches rapidly from v_1 to 0 in a time on the order of R_JC or $Q_0^2=25$ in our dimensionless system. With the junction trapped in a potential minimum, the voltage on the external capacitor then decays to 0 with a time constant of R_sC_b or $Q_0^2/\rho=250$ time units. Thus, in contrast to switching from the 0 to the 1 state, the reverse process shows two distinct time constants: a short one for the junction voltage and a long one for the voltage on the external capacitor.

The dynamics of the switching processes shown in Fig. 15 give important clues to the lifetimes $\tau_\pm$, τ_0, and τ_1. General arguments show that escape from a basin of attraction induced by white Gaussian noise is thermally activated in the limit of low temperatures.[39] Thus, for low temperatures, there exist activation energies $\epsilon_\pm$, ϵ_0, and ϵ_1 such that $\tau_\pm=a_\pm\exp(\epsilon_\pm/\Gamma)$, $\tau_0=a_0\exp(\epsilon_0/\Gamma)$, and $\tau_1=a_1\exp(\epsilon_1/\Gamma)$, where the prefactors $a_\pm$, a_0, and a_1 are at most weakly dependent on temperature compared to the exponential factors. From the dynamics of the

phase-slip process shown in Fig. 15(a) that determines $\tau_{\pm}$, we conclude that the external shunt plays only a minor role. Because the time constant for charging C_b is much longer than the duration of the phase-slip event, v_b does not change significantly during the event, and the energy required to escape from a potential minimum is not affected by the external shunt. Thus, the phase-slip problem reduces approximately to that of escape from a washboard potential of the form given by Eq. (8), and we anticipate that

$$\epsilon_{\pm} \approx \Delta u_{\pm} , \tag{41}$$

as in the RCSJ model. The dynamics of the plasma oscillations that build to create an escape event are, however, affected by the external shunt, since $Q(\omega_p)$ is determined by the parallel combination of R_J and R_s. This effect modifies the prefactor $a_{\pm}$ from that given by Eq. (12) for the RCSJ model, as will be discussed in Sec. V.

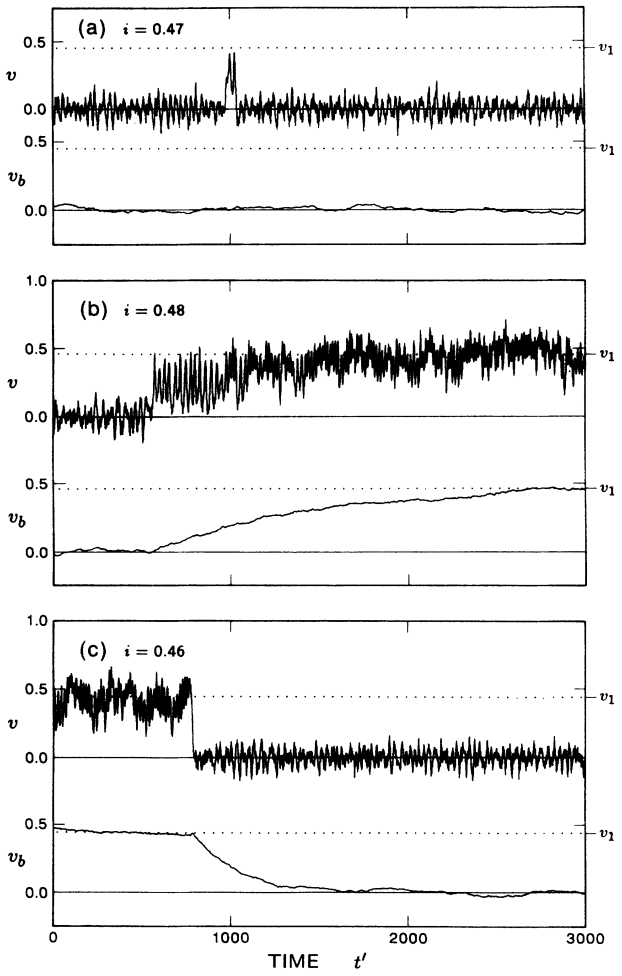

FIG. 15. Voltages on the junction and external capacitance, v and v_b, as a function of time for noise-induced transitions in the system of Fig. 2(b) with $Q_0=5$, $Q_1=2$, $\rho=0.1$, and $\Gamma=0.1$. Frame (a) shows a phase-slip event in which the junction phase increases by 4π at $i=0.47$, frame (b) shows a transition from the 0 state to the 1 state at $i=0.48$, and frame (c) shows a transition from the 1 state to the 0 state at $i=0.46$.

In contrast to phase-slip events, the dynamics of switching from the 0 state to the 1 state that determine τ_0 involve the external shunt in an essential way. Because escape to the 1 state requires noise energy in addition to that needed for escape from a potential minimum, we must have $\epsilon_0 > \epsilon_+$. However, the complexity of the escape process, involving the possibility of retrapping over the long time required to charge C_b, has prevented the development of simple approximations for a_0 and ϵ_0.

A much simpler situation results for switching from the 1 state to the 0 state. As with phase-slip events, the external shunt plays only a minor role in the process of escape from the 1 state. In this process, the junction phase is trapped at a potential minimum in a time much shorter than that required to discharge the external capacitance, as shown in Fig. 15(c). Thus, the energy that must be absorbed by the noise source to stop motion down the washboard includes only that stored in the junction capacitance. On this basis, the activation energy for the trapping process is expected to be on the order of $\frac{1}{2}CV_1^2$ or, in dimensionless notation,

$$\epsilon_1 \approx \tfrac{1}{2}Q_0^2(i-i_{r0})^2 , \tag{42}$$

as for the RCSJ model. The prefactor a_1, on the other hand, probably differs from the RCSJ result of Eq. (14), because, as will be discussed in Sec. VII, the damping at the Josephson frequency is relevant to the trapping process.

Although Eqs. (41) and (42) for $\epsilon_{\pm}$ and ϵ_1 have not been fully verified, they correctly suggest how the model parameters can be modified to produce I-V curves that qualitatively match our experimental results. For the case shown in Fig. 13, overlap between the phase-diffusion and quasiparticle branches occurs only within narrow ranges of both dc bias and temperature. The I-V curves shown in Figs. 13(b) and 13(c) for $\Gamma=0.08$ and $\Gamma=0.1$, are, in fact, near the ends of the temperature range in which phase diffusion overlaps the quasiparticle branch for a dwell time of 10^7 units. At $\Gamma=0.05$, only a few phase-slip events are observed during the dwell time at the switching bias i_s and a phase-diffusion voltage is essentially absent from the I-V curve. On the other hand, at $\Gamma=0.14$, there is no bias point at which the lifetimes τ_0 and τ_1 are both greater than 10^7 units and the I-V curve is nonhysteretic. Thus, for the parameter set used in Fig. 13, phase diffusion overlaps the quasiparticle branch for a temperature range that spans less than a factor of 3 and the overlap, $i_s - i_r$, is always smaller than i_r for I-V curves showing a significant phase-diffusion voltage. This situation contrasts with the experimental I-V curves of Figs. 1 and 4 where the coexistence of phase diffusion and hysteresis is robust, with $i_s \gg i_r$ over more than a factor of 3 in temperature. Moreover, the experimental I-V curves display a finite slope at the origin, a feature that is entirely absent from Fig. 13 in the temperature range where the curves are hysteretic.

To obtain theoretical I-V curves with a finite slope at the origin, the lifetime $\tau_{\pm}$ at $i=0$ must be short enough that many phase-slip events occur during the dwell time. Given that $\tau_{\pm} = a_{\pm}\exp(\epsilon_{\pm}/\Gamma)$ and $a_{\pm}$ is on the order of

$1/\omega_p, \tau_\pm$ will be short provided that Γ is on the order of or greater than $\epsilon_\pm$. Since $\epsilon_\pm = 2$ at $i = 0$ according to Eqs. (13) and (41), we require relatively high temperatures, values of Γ on the order of 2, to obtain a finite slope at the origin. As argued above, the resulting phase-diffusion branch is expected to extend to bias levels no higher than i_m. To obtain an overlapping quasiparticle branch, τ_1 must be long compared to the dwell time at bias levels below i_m. This condition translates into the minimum requirement that the activation energy ϵ_1 be much larger than Γ at $i = i_m$. Combining Eqs. (39), (40), and (42), we obtain

$$\epsilon_1(i_m) \approx \frac{8}{\pi^2}\left[\frac{Q_0}{Q_1} - 1\right]^2 , \tag{43}$$

from which it follows that Q_0 should be chosen much greater than Q_1 to ensure hysteresis. This result confirms the idea that overlap between the phase-diffusion and quasiparticle branches results when the damping is much greater at the plasma frequency than at low frequencies.

In selecting a parameter set that meets the condition $\epsilon_1(i_m) \gg \Gamma$ for $\Gamma = 2$, we have chosen the case $Q_0 = 100$, $Q_1 = 10$, and $\rho = 0.1$, for which $\epsilon_1(i_m)$ is 65.6, as opposed to 1.8 for the parameters of Fig. 13. Accurate numerical evaluation of i_m and i_{r0} for this case yields 0.1267 and 0.0260, as compared with the values 0.1273 and 0.0127 obtained from Eqs. (39) and (40). These results confirm the accuracy of Eq. (39) for i_m in the limit of large Q_1 and show that Eq. (40) for i_{r0} is no more than a rough approximation. *I-V* curves for this higher-Q case, shown in Fig. 16, are much as anticipated. They show a large region of hysteresis between the phase-diffusion and quasiparticle branches that persists over more than a factor of 4 variation in temperature. Most significantly, these curves show a finite slope at the origin. Indeed, the curves shown in Fig. 16 are qualitatively similar to the experimental *I-V* characteristics of Figs. 1 and 4 in almost all respects, including the fact that the switching current is much less than the ideal critical current. This qualitative agreement suggests that the simple model of Fig. 2(b) includes all of the basic elements necessary to understand our experimental results. However, attempts to obtain quantitative agreement between our experiment and models of this type proved unsuccessful. In the next

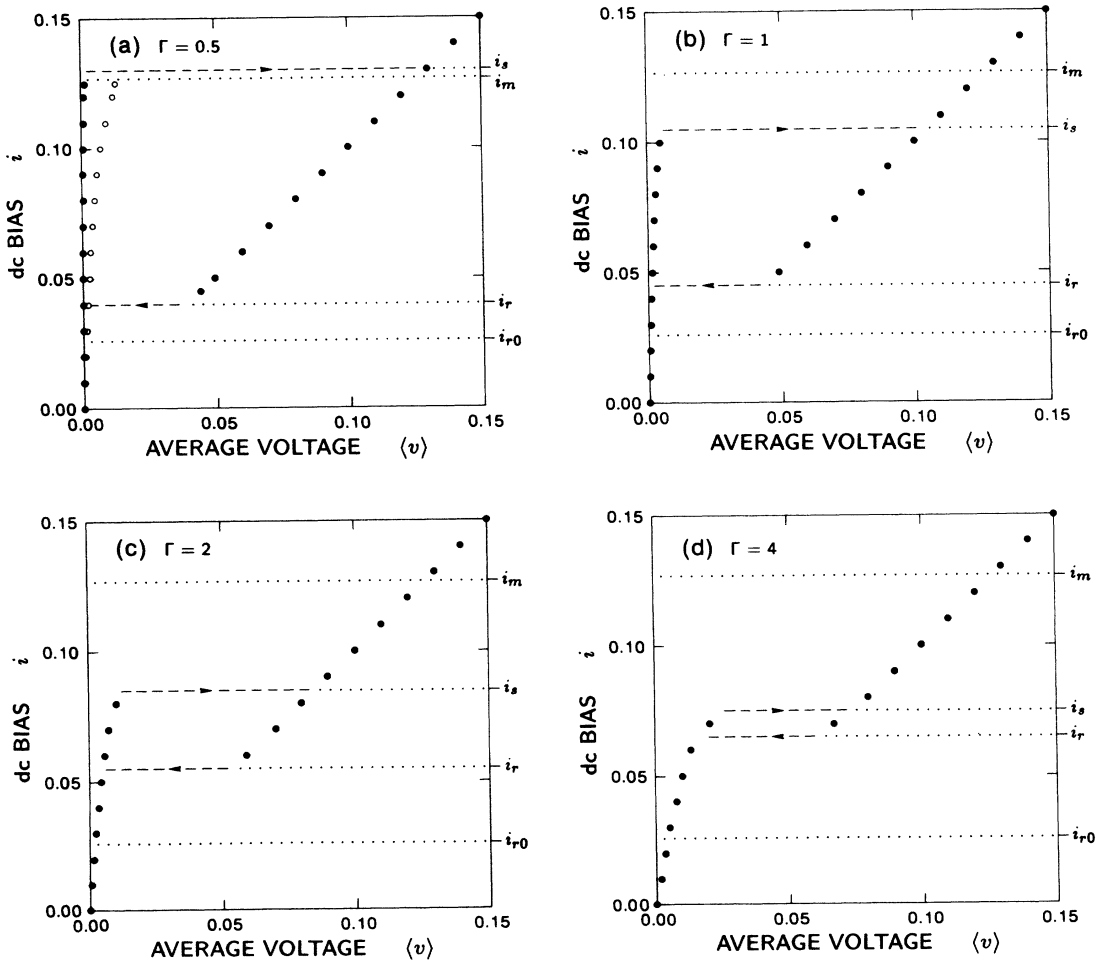

FIG. 16. Noise-affected *I-V* curves for the case $Q_0 = 100$, $Q_1 = 10$, and $\rho = 0.1$ at the temperatures (a) $\Gamma = 0.5$, (b) $\Gamma = 1$, (c) $\Gamma = 2$, and (d) $\Gamma = 4$. Voltages were calculated through Monte Carlo simulations using an averaging time of 10^8 units. The open circles in frame (a) show the voltage of the phase-diffusion state multiplied by a factor of 10.

section we describe a more accurate model that provides such quantitative agreement.

IV. EXPERIMENTAL MODEL

Our experiments used two microcircuit samples of the type sketched in Fig. 3. Each microcircuit, fabricated on a silicon substrate, included a small-area $Nb/NbO_x/Pb$-In-Au edge junction and two Ni-Cr isolation resistors. Experiments were performed in pumped liquid helium over the temperature range from 1.27 to 4 K. A shielded cryoprobe and cold low-pass filters in the dc leads were used to eliminate noise from the room-temperature environment.[32] In discussing the circuit model for this experiment, we consider first the junction and then the external loading.

The edge junctions of both samples measured approximately 0.1 by 1 μm^2 and had nearly identical quasiparticle tunneling characteristics. In particular, the current rise at the gap voltage was approximately 70 nA for both junctions (cf. Fig. 1). For this reason, the parameter values of the junction model were assumed to be the same for both samples. The chosen model consists of the four circuit elements at the right side of Fig. 2(c): an ideal Josephson element of critical current I_0, a shunt capacitance C, a voltage- and temperature-dependent resistive shunt R_J, and a current source I_n representing the Johnson noise of R_J. Due to strong-coupling effects in niobium and lead,[40] I_0 is expected to be about 0.7 times the current rise at the energy gap or about 50 nA. From this nominal value for the critical current and the junction dimensions, its capacitance C is estimated to be roughly 20 fF based on measurements of the specific capacitance of similar junctions.[41] The junction's plasma frequency is thus about 14 GHz.

Because the effects of interest here are sensitive to damping, special attention was given to modeling the temperature and voltage dependence of the quasiparticle conductance represented by R_J. This conductance was measured experimentally near zero voltage by suppressing the Josephson current with a magnetic field. Typical experimental results are shown by the solid lines in Fig. 17 for 2.9, 3.4, and 4 K, temperatures in the range for which the damping due to quasiparticle conduction is most important. As Fig. 17 shows, the quasiparticle current decreases rapidly with temperature: the resistance at the origin of the I-V curve increases from 170 to 580 kΩ as the temperature decreases from 4 to 2.9 K. This resistance is about 4 MΩ at 2 K and rapidly approaches the 20 MΩ dc resistance of the external load at lower temperatures. Thus, the quasiparticle current is most significant at temperatures above 2 K and need be accurately modeled only at these higher temperatures. Moreover, because the phase-diffusion branch is limited to voltages below about 0.05 mV, where the quasiparticle current is proportional to voltage, a simple resistor is an adequate model for calculating phase-diffusion effects. In this low-voltage region, we can fit the measured quasiparticle current within a few percent for temperatures between 3 and 4 K using the expression,

$$I_{qp}=G_1 V \exp(-E/kT) , \tag{44}$$

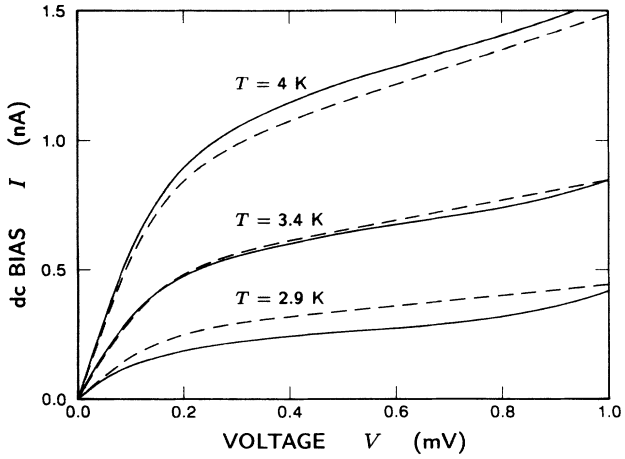

FIG. 17. Quasiparticle current as a function of voltage at 2.9, 3.4, and 4 K. Solid lines plot the experimental result for sample B obtained by suppressing the Josephson current with a magnetic field. Dashed lines show the fit obtained with Eq. (45).

with $G_1^{-1}=6.76$ kΩ and $E=1.1$ meV. However, to obtain accurate results for the return current, which involves switching from the quasiparticle branch at voltages up to 0.3 mV, we must account for the nonlinear relation between I_{qp} and V at higher voltages. For this reason, we adopt the extended parametrization,

$$I_{qp}=[(G_1-G_2)V_0\tanh(V/V_0)+G_2 V]\exp(-E/kT) , \tag{45}$$

with $G_2^{-1}=61$ kΩ and $V_0=0.15$ mV. Equation (45) reduces to Eq. (44) at low voltages and fits the experimental data within a few percent in this region. The fit at higher voltages is less exact but captures the gross behavior very well, as indicated in Fig. 17. In our Monte Carlo simulations we used Eq. (45) to evaluate the quasiparticle current based on the instantaneous junction voltage V.

In modeling the intrinsic noise of the junction, we include only the Johnson noise of the quasiparticle conductance. This noise is represented by the current source I_n in Fig. 2(c) which is taken to be a Gaussian random number generator with 0 mean and variance $\langle I_n^2\rangle=2kT\, dI_{qp}/dV/\Delta t$ in our simulations. Here Δt is the time step used in integration and

$$dI_{qp}/dV=(G_1-G_2)\operatorname{sech}^2(V/V_0)+G_2 , \tag{46}$$

is the differential conductance of the quasiparticle curve, which depends on the instantaneous voltage.

In modeling the external cricuit, we must account for loading due both to the circuit that supplies the dc bias and to the circuit that monitors the voltage. As Fig. 3 suggests, these two circuits are similar: each includes an isolation resistor, a capacitance associated with the leads to the room-temperature environment, and a terminating resistor (either the internal impedance of the current source or the input impedance of the voltage amplifier). To simplify the model, we combine these two circuits into a single circuit in which the isolation resistors, lead capacitances, and terminating resistors are replaced by

their parallel combinations. In Fig. 2(c), these parallel combinations are represented by R_s, C_b, and R_b, respectively. As we discuss presently, there is a distributed parasitic capacitance associated with each isolation resistor and for this reason R_s is broken into M segments R_{si} to allow the addition of $M-1$ intervening capacitors C_{si} to ground. A separate current source I_{ni} is included to account for the Johnson noise of each segment of the isolation resistor. In our simulations these noise sources are taken to be Gaussian random number generators with zero mean and variance $\langle I_{ni}^2 \rangle = 2kT/R_{si}\,\Delta t$. Finally, the model includes a voltage source V_e which together with R_b defines the bias current I.

Nominal values for R_s, C_b, and R_b were assigned on the basis of direct measurements. For our apparatus the lead capacitance C_b was approximately 10 pF and the internal resistance of the current source R_b was 20 MΩ in all experiments. On the other hand, the isolation resistance R_s, determined by the parallel combination of the Ni-Cr resistors on the microcircuit, was different for the two samples studied. For sample A, each resistor measured 4.5 nm thick by 1.5 μm wide by 1.5 mm long and had a resistance of 300 kΩ. The resistors of sample B were similar to those of sample A but were one-third as long and had one-third the resistance. Taken in parallel, these Ni-Cr resistors yield isolation resistances of $R_s = 150$ kΩ for sample A and $R_s = 50$ kΩ for sample B.

The distributed parasitic capacitance C_s associated with the isolation resistors was evaluated by calculating the microwave impedance at the junction terminals due to the antenna structure formed by one isolation resistor and the ground wire. Computer simulations based on Hallen's method,[42] including all electromagnetic and retardation effects, showed that the radiation resistance and inductance of the isolation resistor are negligible in comparison to its resistance but that the distributed capacitance between the isolation resistor and the ground wire is significant at microwave frequencies. This capacitance is uniformly distributed along the resistor and has a value per unit length of approximately $\frac{1}{4}(1+\epsilon)\epsilon_0$, where $\epsilon = 11.8$ is the dielectric constant of the silicon substrate. When the capacitances of the two isolation resistors are combined in parallel, the total parasitic capacitance C_s of sample A is 80 fF and that of sample B is 26.7 fF.

To understand the effect of the external loading in the experimental circuit model, we again consider a frequency-dependent quality factor defined by

$$Q(\omega) = [2eI_0C/\hbar G^2(\omega)]^{1/2}\,, \tag{47}$$

where G is the real part of the admittance shunting the ideal Josephson element. This quality factor is plotted in Fig. 18 as a function of frequency for the circuit models representing samples A and B at a temperature of 2 K. We consider first the case of sample A, for which various critical frequencies are indicated at the top of the figure. At frequencies below about 30 MHz, the parasitic capacitance C_s is an effective open and the circuit model reduces essentially to that considered in Sec. III. In fact, to the extent that R_b is much greater than R_J (in the present case $R_b = 20$ MΩ and $R_J = 4$ MΩ), the shunt conductance in this low-frequency region is precisely that given by Eq. (37). Thus, at frequencies below about 10 kHz, the quality factor is roughly determined by R_J alone and, at frequencies between 100 kHz and 30 MHz, it is determined by $R_\parallel = (R_J^{-1} + R_s^{-1})^{-1}$, the parallel combination of R_J and R_s. According to Eq. (37), the transition between these regions of constant Q begins at $\omega = \sqrt{R_\parallel/R_J}/R_sC_b$ (20 kHz) and is basically complete at $\omega = 1/R_sC_b$ (106 kHz).

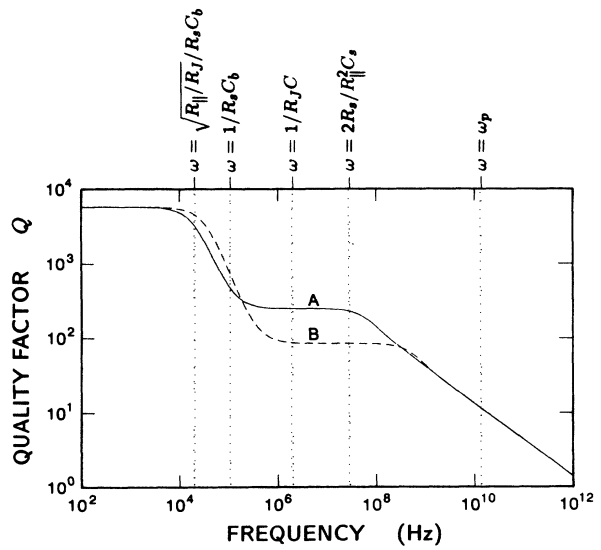

FIG. 18. Quality factor as a function of frequency for the models representing sample A (solid line) and sample B (dashed line) at a temperature of 2 K. The quasiparticle current is taken in the limit of low voltage, and R_J, as defined by Eq. (44), is 4 MΩ. Critical frequencies indicated at the top of the figure apply to sample A.

At frequencies above 30 MHz, the effect of the distributed capacitance C_s cannot be ignored and Eq. (37) is not valid. In this regime, the shunt admittance is dominated by conduction through some fraction of R_s that is shorted to ground through C_s. Considered from the junction's point of view, high-frequency currents propagate down the resistance and capacitance ladder that represents the isolation resistor only to the point where the accumulated capacitance is sufficient to provide a return path. At higher frequencies, this distance is smaller and hence the effective shunt resistance is smaller. This effect explains why Q decreases monotonically with increasing frequency above 30 MHz. Because only the portion of the ladder closest to the junction is active at high frequencies, we can compute its conductance by assuming that the ladder is infinite in length. This strategy yields the simple formula,

$$G(\omega) = \sqrt{\omega C_s/2R_s}\,, \tag{48}$$

which accurately predicts the quality factor plotted in Fig. 18 at frequencies above 100 MHz. The transition between Eqs. (37) and (48) for the conductance occurs roughly at the frequency $\omega = 2R_s/R_\parallel^2 C_s$, where these two expressions are equal, or 20 MHz in the present case.

The admittance of the ladder representing R_s and C_s

also includes an imaginary part, equal to the real part given by Eq. (48), that adds to the imaginary admittance of the junction capacitance C. However, in the limit of high frequencies the contribution of the ladder to the imaginary part of the admittance is small compared to ωC and, in the present case, the plasma frequency of the junction is given to a good approximation by $\omega_p = \sqrt{2eI_0/\hbar C}$.

The quality factor for sample B differs somewhat from that of sample A because R_s and C_s are smaller by a factor of $\frac{1}{3}$. However, for frequencies below 10 kHz, where the damping is determined by R_J, and for frequencies above 300 MHz, where the damping is determined by a fraction of R_s close to the junction, the quality factor is the same for both samples. As a consequence, features of the I-V curve that depend only on the damping at zero frequency or at the plasma frequency are the same in both samples, as is discussed further in Secs. V and VII.

In calculating the quality factor plotted in Fig. 18, the isolation resistance R_s and its distributed capacitance C_s were broken into $M = 1000$ equal parts to ensure an accurate representation of the external load at high frequencies. However, a much more efficient representation of this load is required to enable the extensive Monte Carlo computations presented here. If R_s and C_s are divided uniformly such that $R_{si} = R_s/M$ and $C_{si} = C_s/M$, as in the computation of Q, then the discrete-component ladder is an accurate model for frequencies up to $1/R_{si}C_{si} = M^2/R_sC_s$. By choosing $M = 1000$, we ensure that the ladder is accurate for frequencies up to 10 THz. In our Monte Carlo simulations, on the other hand, it is sufficient that the damping be accurately represented only for frequencies below about 5 times the plasma frequency, or 70 GHz. This relaxed requirement reduces the ladder to about 70 sections.

The ladder can be further simplified by noting that the high-frequency oscillations of significance are generated by the Josephson element and do not propagate very far along the isolation resistor. Thus, portions of the ladder far from the junction need not be modeled as accurately as those near the junction. On this basis, the ladder was reduced to five resistors and four capacitors with the component values listed in Table II. The chosen resistance values increase geometrically section by section as one moves away from the junction and the total resistance is equal to the measured R_s. The capacitor values are taken as the geometric mean of the capacitances associated with the neighboring resistor sections. With the time constant $R_{s1}C_{s1}$ of the first section selected to give a cutoff frequency of about 70 GHz, the resulting ladder of five resistors and four capacitors provides an adequate representation of the isolation resistor and its distributed capacitance, as determined by comparing the junction dynamics with a fully accurate model. In this way, we arrive at a model of the experiment that requires only four additional state variables (the voltages on the capacitors C_{s1} through C_{s4}) beyond the three required for the simple frequency-dependent model of Fig. 2(b). The relative simplicity of this circuit makes feasible the extensive Monte Carlo simulations presented in the following sections.

Table II summarizes all parameter values used in our simulation of the experiment. As this table reiterates, the parameters used to describe samples A and B are identical, with the exception of those related to the isolation resistors. Thus, the fact that agreement between simulation and experiment spans both samples, as shown in Fig. 4, confirms the importance of accurately modeling the external loading. Even more noteworthy, however, is the fact that this agreement was obtained using the nominal parameter values derived in this section without reference to the phase-diffusion branch of the experimental I-V characteristic.

V. PHASE-DIFFUSION RESISTANCE

The process of phase diffusion, which is modeled by the Brownian motion of a particle in a tilted washboard potential, gives rise to a finite voltage as the particle moves down the washboard in fits and starts. For thermal energies kT comparable to the Josephson coupling energy E_J, phase diffusion yields an I-V curve with a finite slope at the origin in place of the usual zero-resistance branch. The resistance R_0 at the origin is an easily measured experimental parameter that can be used to quantify phase diffusion in this temperature regime. Using Monte Carlo simulations as a guide, we examine in this section the physical processes that determine R_0 and develop a simple formula for its evaluation.

The temperature dependence of R_0 is shown in Fig. 19 for samples A and B. In this figure we plot R_0T versus $1/T$ to facilitate comparison with theory. Experimental results for R_0 are plotted as circles and Monte Carlo results, obtained from average voltage values computed at low dc bias, are plotted as squares connected by a solid line to guide the eye. The agreement between experiment and simulation evident in Fig. 19 is excellent in view of the fact that only one circuit parameter, the critical current I_0, was adjusted to fit the experimental data and the adjusted value is fully consistent with the current step at the energy gap. Based on this agreement, we assume in the following discussion that the detailed dynamics of the phase-diffusion process are well represented by the Monte Carlo simulations.

TABLE II. Nominal parameters used to model samples A and B in Monte Carlo simulations.

Samples	I_0 (nA)	C (fF)	G_1^{-1} (kΩ)	G_2^{-1} (kΩ)	E (meV)	V_0 (mV)	R_b (MΩ)	C_b (pF)	
A and *B*	50	20	6.76	61.0	1.1	0.15	20	10	
	R_{s1} (kΩ)	R_{s2} (kΩ)	R_{s3} (kΩ)	R_{s4} (kΩ)	R_{s5} (kΩ)	C_{s1} (fF)	C_{s2} (fF)	C_{s3} (fF)	C_{s4} (fF)
A	1.637	4.535	12.56	34.81	96.45	1.453	4.026	11.15	30.90
B	1.636	3.257	6.485	12.91	25.71	1.232	2.454	4.886	9.730

Two approximate analytic results for R_0 are plotted by dashed lines in Fig. 19. Both of these approximations are based on a scenario suggested by Fig. 5 in which the system spends significant periods of time trapped in a potential minimum but occasionally escapes and traverses one or more wells before being retrapped. Applying the Josephson relation $V=(\hbar/2e)d\phi/dt$ to this situation, we obtain for the average voltage,

$$\langle V\rangle=\frac{h}{2e}\left[\frac{\langle N_+\rangle}{\tau_+}-\frac{\langle N_-\rangle}{\tau_-}\right], \tag{49}$$

where τ_+ and τ_- are the mean times for escape from a potential minimum in the $+\phi$ and $-\phi$ directions and $\langle N_+\rangle$ and $\langle N_-\rangle$ are the mean numbers of wells traversed after such escape events. In Fig. 19, the theory corresponding to the line with the longer dashes makes the conventional assumption,[5,13,14] valid in the limit of low temperature, that $N_+=N_-=1$. However, in the experiment considered here, the temperature is high enough that escape events frequently lead to a phase slip of several revolutions. When such multiple-well phase-slip events are accounted for, we obtain the curve plotted with the shorter dashes in Fig. 19, which agrees well with both the experiment and the Monte Carlo simulations.

The theoretical curves of Fig. 19 are derived by reducing the circuit of Fig. 2(c) to an approximate RCSJ model. This reduction is based on the observation that phase diffusion involves motion almost exclusively at frequencies near the plasma frequency. The dynamical processes important to phase diffusion are the noise-induced plasma oscillations that build to produce an escape event and the Josephson oscillations that occur as the system traverses the washboard potential before retrapping. Because the junction voltage remains small during the period of phase slippage, these Josephson oscillations are at a frequency close to ω_p [cf. Figs. 5 and 15(a)]. Thus, all of the dynamical effects relevant to phase diffusion occur at frequencies near the plasma frequency. Because the reactance at ω_p contributed by the external capacitors C_b and C_s is, as noted in Sec. IV, small compared to the junction capacitance, the only energy-storage elements important to the dynamics of phase diffusion are the ideal Josephson element and the junction capacitance. The external circuit does, however, determine the damping at the plasma frequency and to account for this we take the resistance shunting the junction to be $R_p\equiv 1/G(\omega_p)$. Since damping at other frequencies is not important to phase diffusion, use of this frequency-independent resistance is a good approximation. Thus, we expect the dynamics of phase diffusion to be well represented by a RCSJ model in which the critical current and junction capacitance are chosen to be the nominal values listed in Table II and the shunt resistance is R_p.

To evaluate R_p for samples A and B, we note that the plasma frequency is in a range for which Eq. (48) is valid. Thus, $R_p=\sqrt{2R_s/\omega_p C_s}$ and, because the resistance and capacitance per unit length are the same for the isolation resistors of both samples, R_p is 16.4 kΩ in both cases.

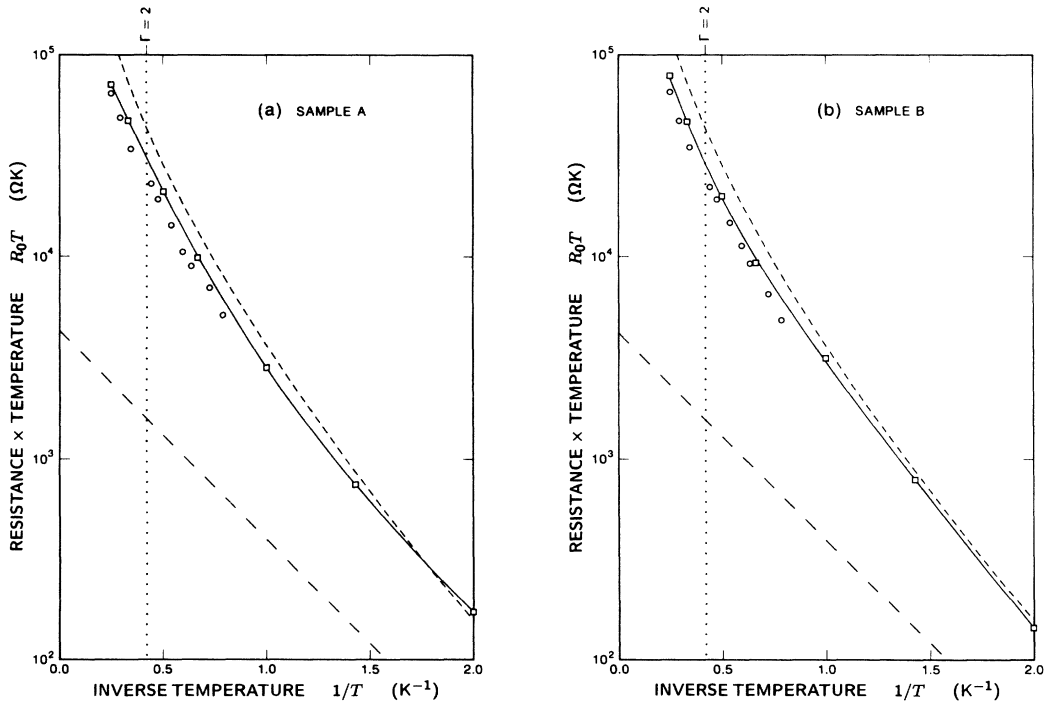

FIG. 19. Product of resistance at the origin and temperature as a function of inverse temperature for (a) sample A and (b) sample B. Experimental points are shown by circles and points obtained through Monte Carlo simulations are plotted as squares. The Monte Carlo points are connected by a solid line as a guide to the eye. Two analytic approximations, Eqs. (51) and (65), are plotted as dashed lines with long and short dashes, respectively.

The corresponding quality factor is $Q_p \equiv Q(\omega_p) = 28.7$. Because all of the parameters entering our reduced model are identical for samples A and B, the model predicts that the phase-diffusion resistance R_0 will be the same for both samples. This prediction is confirmed by Fig. 19, which shows virtually identical results for the two samples in both the experiments and the simulations.

In developing the theoretical expressions for R_0 plotted in Fig. 19, we make extensive use of Monte Carlo simulations to check intermediate results. The use of simulations to determine quantities such as $\tau_\pm$ and $\langle N_\pm \rangle$ requires that we distinguish the time intervals during which the system is trapped in a potential well from those in which it is moving from well to well in the $+\phi$ or $-\phi$ direction. That is, we need to assign all portions of a Monte Carlo time record, such as that shown in Fig. 5, to one of three system states: the 0 state (trapped in a well), the + state (motion in the $+\phi$ direction), or the − state (motion in the $-\phi$ direction). The way in which these assignments are made defines the quantities $\tau_\pm$ and $\langle N_\pm \rangle$. Although inspection of Fig. 5 suggests that the 0, +, and − states are distinct and well defined, they cannot be distinguished on the basis of the system's location in state space. The relevant state-space diagram is one with a topology like that of either Fig. 9(a) or Fig. 14 and, throughout the process of phase diffusion, the system is always found within the basin of one potential minimum or another. However, reasonable state assignments can be made if the history of the system is taken into account. In particular, the following rules, defining transitions between the states, allow an unambiguous determination of the system's state at all times.

(1) The system enters the $\pm$ state from the 0 state when ϕ crosses the potential maximum located in the $\pm\phi$ direction from the currently occupied minimum.

(2) The system enters the 0 state from the $\pm$ state when $d\phi/dt$ reverses sign.

An example in which these rules are applied to determine the state of the system is shown in Fig. 20. In this figure, unshaded regions correspond to time intervals in which the junction is in the 0 state, with the phase oscillating about a potential minimum, and shaded regions correspond to intervals in which the junction is in the + state or − state, with the phase slipping between minima. Although our rules are to some extent arbitrary, they define intervals in which the phase is trapped or slipping in a useful fashion, consistent with intuition.

Our simplest analytic approximation for R_0 assumes that $N_\pm = 1$ and requires only an estimate for the lifetimes τ_+ and τ_-. Because the RCSJ model is being applied, we expect these lifetimes to be given by Eq. (12). However, this equation was derived for a situation in which the system is initialized with the phase near a potential minimum, as in the switching experiments of Fulton and Dunkleberger[12] where the dc bias is ramped from 0. As a result, the second form given by Eq. (12), valid at higher temperatures, was developed to account for the fact that states near the escape energy are initially unoccupied.[16] Because phase diffusion is a steady-state process, this form is not appropriate to our problem. However, the first form given by Eq. (12) derives from transition-state theory which is based on the assumption of a steady state. Thus, we expect to obtain a good approximation for the lifetimes relevant to phase diffusion simply by extending the first form of Eq. (12) to cover the entire temperature range. Restoring dimensions to this equation and taking the limits $Q_p \gg 1$ and $i \ll 1$ yields

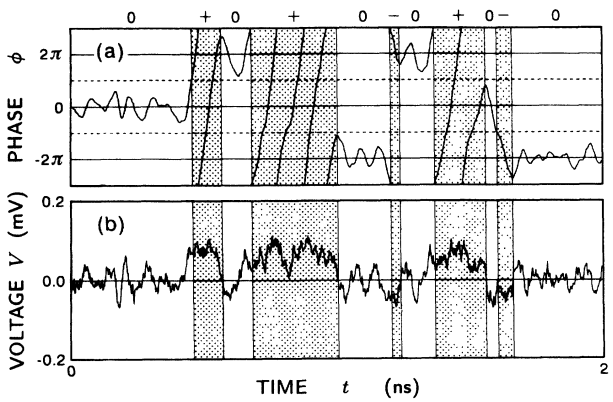

FIG. 20. Calculated time dependence of (a) the phase and (b) the voltage of a junction in the phase-diffusion state corresponding to the experimental situation shown in Fig. 1 for a dc bias of $I = 0.5$ nA. Shaded regions indicate time intervals during which the junction is in the $\pm$ state and unshaded regions correspond to the 0 state.

$$\tau_\pm = \frac{2\pi}{\omega_p (1-i^2)^{1/4}} \exp(\Delta u_\pm / \Gamma)$$

$$(\Gamma \ll \Delta u_\pm,\ Q_p \gg 1,\ i \ll 1)\ . \quad (50)$$

This formula is compared with the Monte Carlo results for $\tau_\pm$ in Fig. 21 for a case corresponding to sample A at zero dc bias. The Monte Carlo results are based on simulations of the full circuit model shown in Fig. 2(c) over a period of 20 μs. The lifetimes τ_+ and τ_- are computed as the total time spent in the 0 state divided by the number of escape events in the $+\phi$ and $-\phi$ directions. The results for τ_+ are plotted as circles and those for τ_- are plotted as squares. Since τ_+ and τ_- should be equal to zero bias, the small differences observed here are indicative of statistical errors resulting from the use of a finite averaging time. The Monte Carlo results are to be compared with Eqs. (12) and (50) which are plotted in Fig. 21 as the dashed and solid lines, respectively. Although both of these formulas are strictly valid at zero bias only for $\Gamma \ll 2$, there is good qualitative agreement between the Monte Carlo simulations and Eq. (50) for temperatures up to $\Gamma \approx 2$. By contrast, Eq. (12) is in poor qualitative agreement with the simulations over the temperature range $4\pi/Q_p < \Gamma < 2$ where the formula assumes a special distribution of junction states rather than the appropriate steady-state distribution. Figure 21 thus confirms the legitimacy of using the transition-state theory to describe phase diffusion over the entire temperature range $\Gamma \ll 2$ and shows that it is accurate within roughly a factor of 2 even for $\Gamma \approx 2$.

Combining Eqs. (49) and (50) with the assumption that

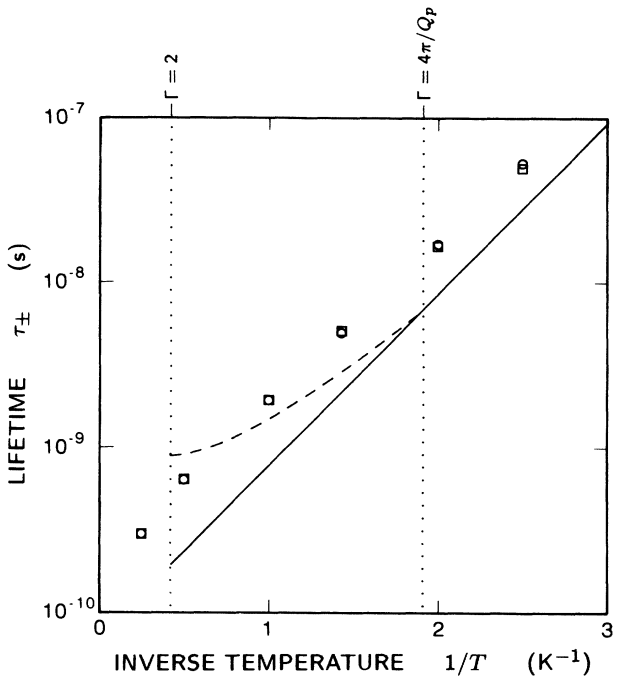

FIG. 21. Mean time for escape from the 0 state as a function of inverse temperature for sample A at zero dc bias. The results of Monte Carlo simulations for τ_+ and τ_-, based on an averaging time of 20 μs, are shown by circles and squares. The analytic results given by Eqs. (12) and (50) are plotted as dashed and solid lines, respectively.

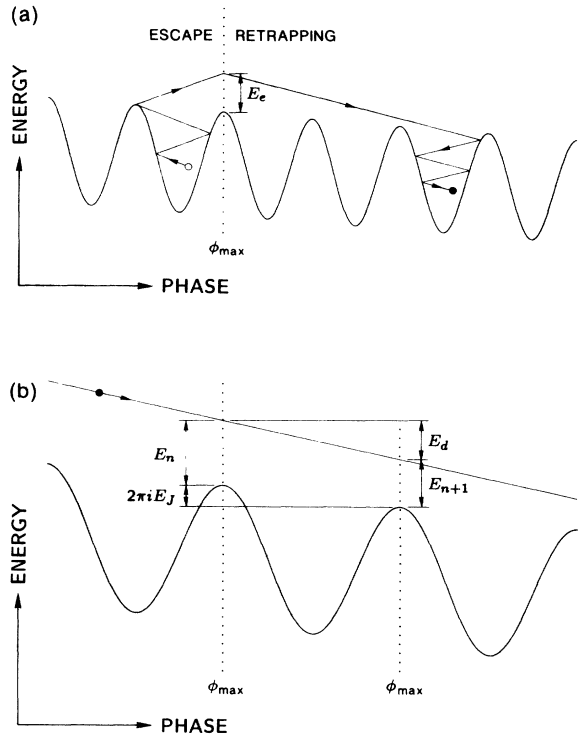

FIG. 22. Energy vs phase for an idealized escape and retrapping event. Frame (a) shows the complete event and frame (b) shows the balance of energy for a single Josephson oscillation during retrapping.

$N_\pm = 1$, we obtain an explicit expression for the average voltage as a function of current that is valid in the limit of low temperature.[5,13,14] Evaluating $d\langle V\rangle/dI$ at $I=0$ for this expression yields the approximate phase-diffusion resistance,

$$R_0 = \frac{2\pi R_p}{Q_p \Gamma} \exp(-2/\Gamma) \quad (\Gamma \ll 2,\ Q_p \gg 1) . \tag{51}$$

This formula, plotted by long dashes, is compared with experiment and simulation for samples A and B in Fig. 19. Although the simulated values of R_0 tend toward those given by Eq. (51) at the lowest temperatures plotted, the discrepancy over the experimental temperature range is typically greater than an order of magnitude. The difficulty with Eq. (51) is that it does not account of the prevalence of multiple-well phase-slip events at the relatively high temperatures of the experiment.

In the remainder of this section, we consider the problem of estimating the average number of wells traversed in a phase-slip event using the RCSJ model. Our approach to this problem is based on an idealized trajectory, shown in Fig. 22(a), in which a phase-slip event is broken into separate escape and retrapping segments. The escape segment ends when the noise-induced plasma oscillations within the initial well build to the point that the system crosses a potential maximum. When escape occurs at $\phi = \phi_{\max}$, the energy of the system will exceed the minimum required for escape by an amount E_e that varies from event to event depending on the thermal noise. In contrast, the retrapping segment of our idealized event is assumed to occur in the absence of noise. Thus, the number of wells traversed is determined entirely by the escape energy E_e and the dynamics of the noise-free system. Estimates of $\langle N_\pm \rangle$ based on this idealized trajectory assume that for a given E_e the number of wells traversed during the retrapping process is, on average, unaffected by thermal noise. To calculate $\langle N_\pm \rangle$, we must determine both the distribution of escape energies E_e produced during the escape segment and the number of wells traversed during the retrapping segment for a given E_e. The latter problem is considered first.

Taking the points $\phi_{\max}$ to be the boundaries between wells of different index n, we define $N_\pm$ to be the difference in index between the starting well and the well in which the system retraps. Because the system necessarily reaches a neighboring well after an escape event, $N_\pm$ can never be less than 1. The number of additional wells traversed depends on the initial escape energy and the rate of energy loss in moving from well to well. If E_n is the extra energy of the system at the point it enters the nth well and motion is in the $+\phi$ direction, then conservation of energy requires that

$$E_{n+1} = E_n + 2\pi i E_J - E_d(E_n) , \tag{52}$$

where $2\pi i E_j$ is the difference in potential energy between one maximum and the next [cf. Eq. (8)] and $E_d(E_n)$ is the energy dissipated in traversing the nth well. Equation (52) is illustrated graphically in Fig. 22(b). In princi-

ple, the total number of wells traversed for a given E_e can be determined by iterative application of Eq. (52) to find the well in which E_n falls below 0 and retrapping occurs. However, to obtain a simple analytic formula, we convert this difference equation to a differential equation,

$$\frac{dE}{dn}=2\pi iE_J-E_d(E)\ , \tag{53}$$

by assuming that n is a continuous variable. Solving Eq. (53) and its companion for motion in the $-\phi$ direction yields an approximate equation for the total number of wells traversed while the energy decays from E_e to 0,

$$N_{\pm}=1+\int_0^{E_e}dE\frac{1}{E_d(E)\mp 2\pi iE_J}\ . \tag{54}$$

In this equation, the 1 accounts for the inevitable slippage of one well and the integral approximates the additional wells traversed.

To obtain an explicit formula for $N_{\pm}$ from Eq. (54), we must evaluate $E_d(E)$, the energy dissipated in the shunt resistance R_p while traversing a single well, given that the well is entered with an extra energy E. By definition, E_d is given by

$$\begin{aligned}E_d(E)&=\frac{1}{R_p}\int_0^{t_w}V^2\,dt\\&=\frac{\hbar}{2eR_p}\int_{\phi_{\max}}^{\phi_{\max}+2\pi}V\,d\phi\ ,\end{aligned} \tag{55}$$

where t_w is the time required to traverse the well and the second form is obtained using the Josephson relation, Eq. (4). Because we are interested primarily in bias levels near zero and low levels of dissipation, a useful estimate of E_d is obtained by approximating the voltage waveform with that for zero bias and zero dissipation. In this case, energy conservation implies that

$$\tfrac{1}{2}CV^2=E+E_J(1+\cos\phi)\ , \tag{56}$$

and the energy dissipated in traversing one well is

$$\begin{aligned}E_d(E)&=\frac{\hbar}{2eR_p}\sqrt{2/C}\int_{-\pi}^{\pi}\sqrt{E+E_J(1+\cos\phi)}\,d\phi\\&\approx\frac{8E_J}{Q_p}[1+(\pi^2/8)E/E_J]^{1/2}\ .\end{aligned} \tag{57}$$

Here, in the final step, the integral is approximated by a closed form that is exact for $E=0$ and differs from the accurate value by no more than 3% for $E>0$. Combining Eqs. (54) and (57) yields

$$\begin{aligned}N_{\pm}=1&+\frac{2Q_p}{\pi^2}\{[1+(\pi^2/8)E_e/E_J]^{1/2}-1\}\\&\pm\frac{iQ_p^2}{2\pi}\ln\left[\frac{\sqrt{1+(\pi^2/8)E_e/E_J}\mp(\pi/4)iQ_p}{1\mp(\pi/4)iQ_p}\right]\ .\end{aligned} \tag{58}$$

Thus, we arrive at an approximate formula for the number of wells slipped for a given escape energy.

The distribution of escape energies is dependent on the noise that produces the escape events. To obtain a rough estimate of this distribution we consider the case of zero dc bias and restrict our attention to a set of idealized escape trajectories. In particular, we assume that escape occurs after a half oscillation within the initial well that begins at $\phi=-\pi$ with $V=0$ and ends at $\phi=\pi$ with $V=\sqrt{2E_e/C}$. If we further assume that the effect of the noise current $I_n(t)$ can be replaced by its average value $\bar{I}_n$ over the interval t_w required to traverse the well, then the escape energy can be written as

$$E_e=2\pi E_J\bar{I}_n/I_0-E_d(0)\quad(E_e>0)\ . \tag{59}$$

In this equation the first term accounts for the energy imparted to the system by the noise source over the half oscillation leading to escape and the second term approximates the damping losses over this half oscillation. The condition in parentheses indicates that Eq. (59) is valid only if it predicts a positive escape energy. Using Eq. (57) to evaluate $E_d(0)$ yields

$$E_e=2\pi E_J(\bar{I}_n-I_m)/I_0\quad(\bar{I}_n>I_m)\ , \tag{60}$$

where $I_m=4I_0/\pi Q_p$ is the minimum average noise current required for escape. Because I_n represents the Johnson noise of the resistance R_p, the probability of an average noise current $\bar{I}_n$ over an interval t_w is

$$P(\bar{I}_n)=\frac{1}{\sqrt{2\pi}\sigma}\exp(-\bar{I}_n^2/2\sigma^2)\ , \tag{61}$$

where the variance σ^2 is

$$\sigma^2=\frac{2kT}{R_pt_w}\ . \tag{62}$$

As a rough estimate for the time t_w required to complete a half oscillation, we take $t_w=2\pi/\omega_p$. This estimate is reasonable because half of a small-amplitude plasma oscillation requires a time of π/ω_p and large-amplitude oscillations require longer times. Using $t_w=2\pi/\omega_p$, which is roughly confirmed by Monte Carlo simulations, we obtain

$$\sigma^2=\frac{kT\omega_p}{\pi R_p}\ . \tag{63}$$

Taken together, Eqs. (60), (61), and (63) completely specify the distribution of escape energies. In principle, these equations could be combined with Eq. (58) to compute the average of $N_{\pm}$ over escape energies. However, the resulting expression is sufficiently complex that we consider instead the rough approximation $\langle N_{\pm}(E_e)\rangle\approx N_{\pm}(\langle E_e\rangle)$. This approximation is accurate in the limit $E_e\ll E_j$ for which $N_{\pm}$ increases linearly with E_e. Evaluation of the average escape energy $\langle E_e\rangle$ from Eqs. (60), (61), and (63) is straightforward and yields

$$\begin{aligned}\langle E_e\rangle&=\frac{2\pi E_J}{I_0}\left[\frac{\int_{I_m}^{\infty}(\bar{I}_n-I_m)\exp(-\bar{I}_n^2/2\sigma^2)d\bar{I}_n}{\int_{I_m}^{\infty}\exp(-\bar{I}_n^2/2\sigma^2)d\bar{I}_n}\right]\\&=\frac{8E_J}{\sqrt{\pi}Q_p}\left[\frac{\exp(-z^2)}{z\,\mathrm{erfc}(z)}-\sqrt{\pi}\right]\ ,\end{aligned} \tag{64}$$

where erfc is the complementary error function[43] and $z=\sqrt{8/\pi Q_p}\Gamma$. We compare this result with Monte Carlo simulations in Fig. 23, which shows the average escape energy as a function of temperature for parameters corresponding to sample A at zero dc bias. Although Eq. (64), plotted as a solid line, falls significantly below the Monte Carlo results, plotted as circles, the two curves are qualitatively similar and appear to approach each other in the limit of low temperature.

As a check on these results for the average escape energy, we note that the thermal energy kT, plotted as a dashed line in Fig. 23, is an upper bound on $\langle E_e \rangle$. This bound is established by a detailed calculation, not presented here, of the average thermal energy of an ensemble of particles in an untilted washboard potential. If we measure the particle energies E using the potential maximum as a zero of energy, then the average thermal energy $\langle E_t \rangle$ of those particles with $E>0$ is always between $\frac{1}{2}kT$ and kT and approaches kT in the limit of low temperature. Thus, kT is an upper bound on the average energy $\langle E_t \rangle$ of particles above the potential maximum under the condition of thermal equilibrium. Because particles just escaping from a well are not fully thermalized, the average escape energy $\langle E_e \rangle$ is necessarily less $\langle E_t \rangle$ and is also bounded by kT. The fact that $\langle E_e \rangle$ is significantly less than kT at the higher temperatures in Fig. 23 is consistent with this picture since complete thermalization at high temperatures cannot be expected to occur in the time required to traverse a single well. In the low-temperature limit, where thermalization should occur more quickly, both the Monte Carlo and analytic results for $\langle E_e \rangle$ appear to approach kT. However, the low-temperature asymptote of Eq. (64) is actually $(\pi/2)kT$, so this equation marginally violates the kT bound on $\langle E_e \rangle$. In spite of this inconsistency, Eq. (64) is roughly accurate and provides a useful estimate of the average escape energy over the range of temperatures of interest here.

The estimate of $\langle N_\pm \rangle$ resulting from the approximation $\langle N_\pm(E_e)\rangle \approx N_\pm(\langle E_e \rangle)$ combined with Eqs. (58) and (64) is compared with Monte Carlo simulations in Figs. 24 and 25. Figure 24 shows $\langle N_\pm \rangle$ as a function of temperature for parameters corresponding to sample A at zero dc bias. The Monte Carlo results for $\langle N_+ \rangle$ and $\langle N_- \rangle$, plotted by circles and squares, respectively, should be identical at zero bias but differ slightly in Fig. 24 due to the finite averaging time. The temperature dependence of the analytic result for $\langle N_\pm \rangle$, plotted by a solid line, is in good agreement with the simulations. Somewhat less accuracy is apparent in the bias dependence of Eqs. (58) and (64), as illustrated in Fig. 25. This figure shows $\langle N_+ \rangle$ and $\langle N_- \rangle$ as a function of dc bias for a temperature of 2 K. Although the analytic and Monte Carlo results for $\langle N_\pm \rangle$ agree well in magnitude near $I=0$, the derivatives $d\langle N_\pm \rangle/dI$, on which the resistance R_0 is critically dependent, differ by roughly a factor of 2. Thus, our analytic result, while in good qualitative agreement with the simulations, is only roughly correct in quantitative terms.

Based on our analytic results for $\langle N_\pm \rangle$ and $\tau_\pm$, Eq. (49) can be used to estimate the average phase-diffusion

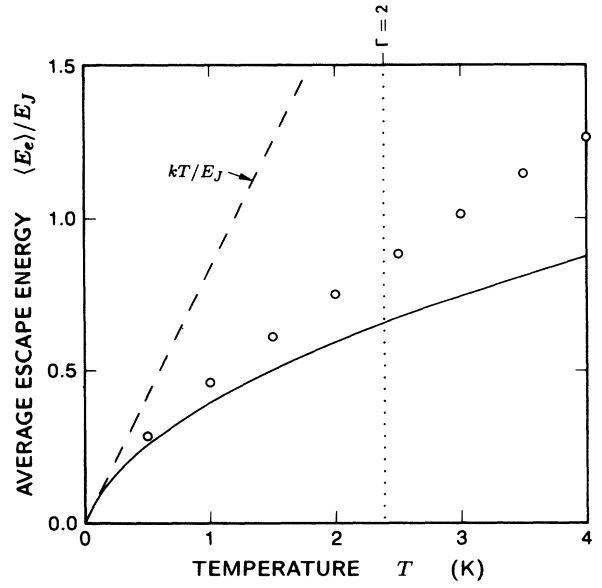

FIG. 23. Average escape energy as a function of temperature for parameters corresponding to sample A at zero dc bias. The results of Monte Carlo calculations based on the full circuit model are plotted as circles, with each circle representing the average escape energy for all phase-slip events in a 20-μs period. Our approximate analytic result for $\langle E_e \rangle$ given by Eq. (64) is plotted as a solid line and, for reference, kT is plotted as a dashed line.

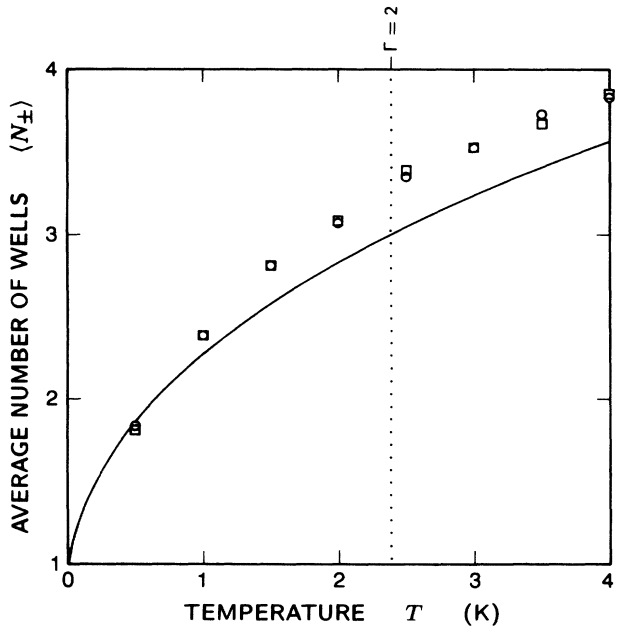

FIG. 24. Average number of wells traversed in a phase-slip event as a function of temperature for parameters corresponding to sample A at zero bias. The results of Monte Carlo simulations based on the full circuit model show the average number of wells slipped in the $+\phi$ and $-\phi$ directions, plotted as circles and squares, respectively, for all phase-slip events in a 20-μs period. The solid line shows the approximation $\langle N_\pm(E_e)\rangle \approx N_\pm(\langle E_e \rangle)$ evaluated using Eqs. (58) and (64).

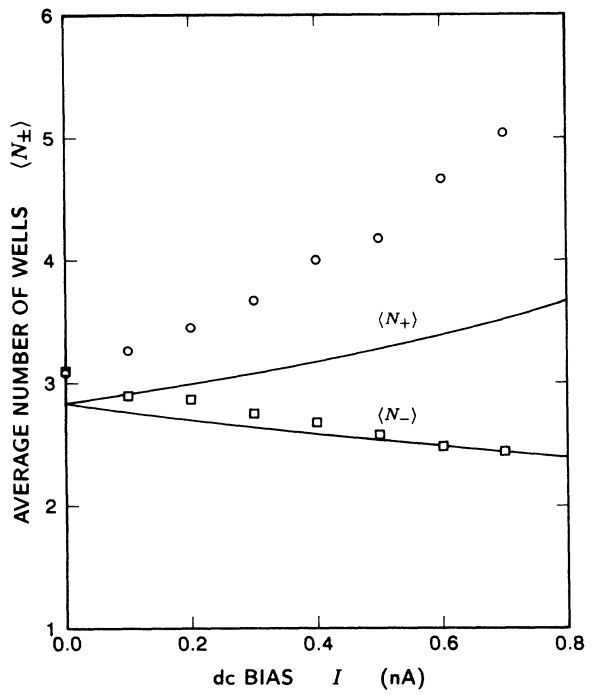

FIG. 25. Average number of wells traversed in a phase-slip event as a function of dc bias for parameters corresponding to sample A at 2 K. The results of Monte Carlo simulations based on the full circuit model show the average number of wells slipped in the $+\phi$ and $-\phi$ directions, plotted as circles and squares, respectively, for all phase-slip events in a 20-μs period. The solid lines show the approximation $\langle N_\pm(E_e)\rangle \approx N_\pm(\langle E_e\rangle)$ evaluated using Eqs. (58) and (64).

voltage as a function of dc bias, including the effect of multiple-well phase-slip events. A straightforward calculation of $d\langle V\rangle/dI$ at $I=0$ yields the phase-diffusion resistance,

$$R_0=\frac{2\pi R_p}{Q_p\Gamma}\exp(-2/\Gamma)\left\{1+\frac{2Q_p}{\pi^2}\times\left[\left[1+\frac{\pi^2\langle E_e\rangle}{8E_J}\right]^{1/2}-1\right]+\frac{Q_p^2\Gamma}{4\pi^2}\ln\left[1+\frac{\pi^2\langle E_e\rangle}{8E_J}\right]\right\}, \tag{65}$$

where $\langle E_e\rangle$ is understood to be evaluated using Eq. (64). This formula for R_0 reduces to Eq. (51) in the limit of low temperatures as expected, since multiple-well phase slips are improbable in this limit. However, at the relatively high temperatures of our experiment, the correction for multiple-well events included in Eq. (65) is substantial. This is illustrated in Fig. 19, where Eq. (65) is plotted as the line with short dashes and Eq. (51) as the line with long dashes. At 4 K, the highest experimental temperature, Eq. (51) underestimates the Monte Carlo value for R_0 by a factor 30 while Eq. (65) overestimates it by a factor of 1.6. We conclude that multiple-well events are important in determining R_0 at high temperatures and are reasonably well accounted for by Eq. (65). Indeed, the accuracy of Eq. (65) in comparison with our Monte Carlo simulations is remarkably good over the entire temperature range of Fig. 19, especially considering the number of simplifying assumptions that entered its derivation. Although this accuracy is to some extent fortuitous in that the error in our estimate of the lifetime apparent in Fig. 21 compensates to some extent for the error in our estimate of $d\langle N_\pm\rangle/dI$ apparent in Fig. 25, there can be little doubt that Eq. (65) captures the essential physics of multiple-well phase-slip events.

As further verification of Eq. (65), we compare it directly with results for the RCSJ model. Since Eqs. (51) and (65) were derived on the basis of the RCSJ model under the assumption that phase diffusion depends only on the damping at the plasma frequency, they can be applied to this model simply by taking $R_p=R_J$ and $Q_p=Q$. These formulas for R_0 are plotted in Fig. 26 by the dashed and solid lines, respectively, for the case $Q=5$. This figure also shows the results of Monte Carlo simulations for $Q=5$, plotted by circles, and the Fokker-Planck results of Vollmer and Risken[17] for $Q\gg1$, plotted by squares. The Monte Carlo points are believed to be accurate within the extent of the circles and serve as a basis of comparison. Equation (51), which neglects multiple-well phase slips, deviates significantly from the Monte Carlo results at $\Gamma=1$ and predicts a phase-diffusion resistance that declines with increasing temperature above $\Gamma=2$.

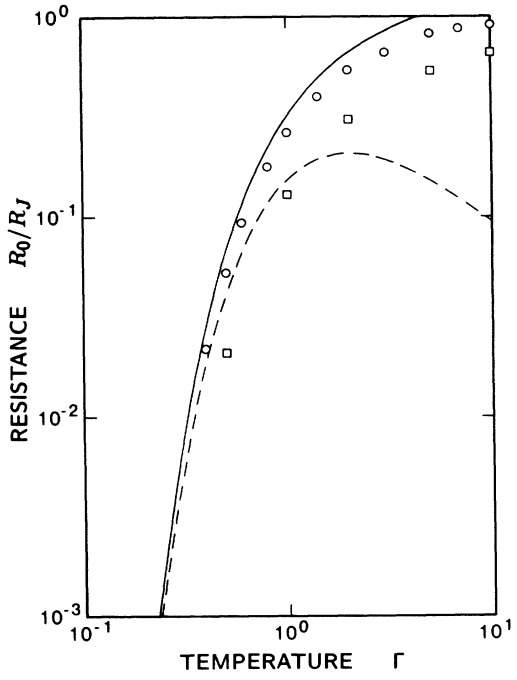

FIG. 26. Phase-diffusion resistance as a function of temperature for the RCSJ model with $Q=5$. Monte Carlo results based on voltages averaged over 10^7 time units are shown by circles. The results of Vollmer and Risken (Ref. 17) obtained by solving the Fokker-Planck equation in the limit of large Q, are shown by squares. Equations (51) and (65) are plotted by dashed and solid lines, respectively.

Equation (65), which accounts for multiple-well phase slips, is much more accurate and differs from the Monte Carlo result by no more than 40% for temperatures up to $\Gamma=10$. However, Eq. (65) fails qualitatively for temperatures above $\Gamma=4.4$ in the sense that it predicts values of R_0 that exceed R_J, an upper bound that should be approached only in the limit of high temperature. In spite of this discrepancy, Eq. (65) is accurate enough to provide a useful estimate of the phase-diffusion resistance for the RCSJ model.

In this section we have shown that multiple-well phase-slip events are an essential element of phase diffusion at high temperatures. Taking multiple-well events into account, we have developed a simple analytic estimate for the phase-diffusion resistance and shown that it agrees well with both experimental and Monte Carlo results. This agreement, obtained for a situation in which the damping is highly frequency dependent, justifies the assumption underlying our analysis that phase diffusion depends only on the damping at frequencies near the plasma frequency. Considering the converse of this relationship suggests that measurements of the phase-diffusion resistance might be used to estimate the effective shunt resistance at the plasma frequency in cases where I_0, C, and T are otherwise known. Our analytic result for R_0 could be particularly useful in this regard because alternative methods of estimation, such as those based on the Fokker-Planck equation or Monte Carlo simulations, are computationally intensive. Thus, Eq. (65) is a potentially valuable tool in the interpretation of the phase-diffusion branch in experimentally measured *I-V* curves.

VI. SWITCHING CURRENT

The switching current I_s is the dc bias at which a junction switches from the zero-voltage branch or the phase-diffusion branch of a hysteretic *I-V* curve to the quasiparticle branch. In the absence of noise, the switching current is equal to the ideal critical current I_0. In the presence of noise, switching generally occurs before the bias reaches I_0 at a point that varies from trial to trial. Thus, a unique value can be assigned to I_s only if we define it as an average of some type. In Sec. II, for example, we defined I_s to be the bias below which half of all switching events occur on average when the bias is ramped from zero at a constant slew rate $|dI/dt|$. Although we will generally be less precise in defining I_s in this section, it is important to keep in mind that noise-induced switching is a statistical event and that the average switch point I_s depends on the slew rate in the case of experimental measurements and the dwell time in the case of simulations at fixed bias levels.

Experimental values of I_s for samples A and B are plotted as a function of temperature in Fig. 27. In our experiments, *I-V* curves were recorded on an *X-Y* plotter over a period on the order of 1 min and the measured switching current was virtually identical from trial to trial. For both samples, the switching current was roughly 2% of the ideal critical current over the temperature range from 1.27±4.0 K. As discussed by Akoh *et al.*[1] and Iansiti *et al.*,[3] the observation of a switching current with small statistical variation that is also a small fraction of I_0 is inconsistent with the predictions of the RCSJ model. For noise levels high enough to cause switching near zero bias, the RCSJ model predicts a large statistical variation in the switch point. Thus, it was known from the outset that our experimental results could not be explained by the simple RCSJ model.

The circuit model of Fig. 2(c) does, however, provide a satisfactory explanation of our experiment. Monte Carlo estimates of the switching current based on this model are shown in Fig. 27 by vertical bars. The top of each bar indicates a bias level at which the junction switched from the phase-diffusion branch in a time less than 40 μs while the bottom indicates a bias level at which the junction remained on this branch for a period greater than 40 μs. As Fig. 27 shows, the agreement between simulation and experiment is excellent for both samples over the entire temperature range. Again, we stress that this agreement results for an entirely nominal set of circuit parameters.

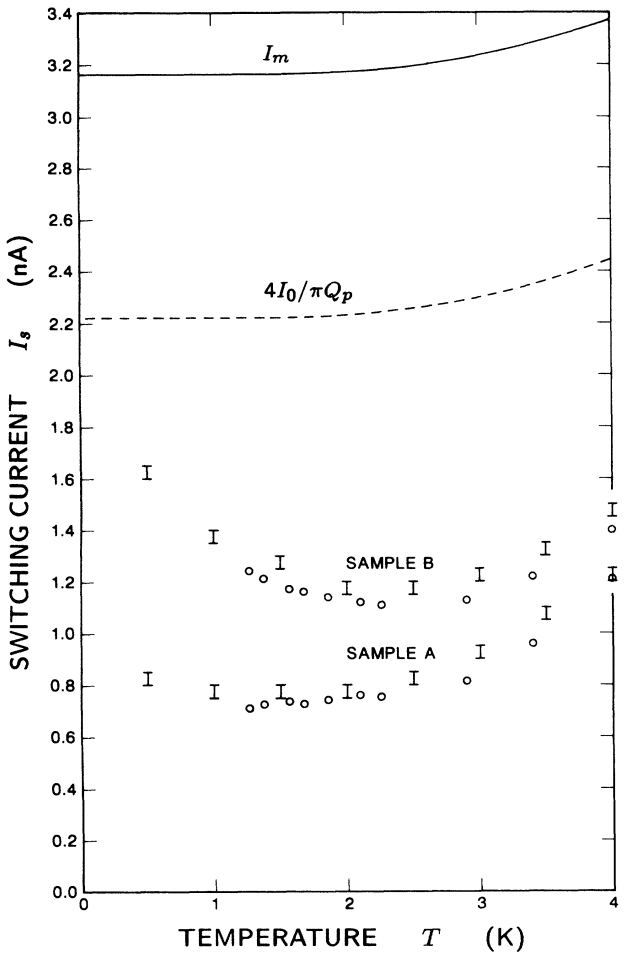

FIG. 27. Switching current as a function of temperature for samples A and B. Circles show experimental results and vertical bars show Monte Carlo results based on the circuit model of Fig. 2(c). The tops and bottoms of these bars indicate bias points at which switching did and did not occur, respectively, for a dwell time of 40 μs. For reference, the bias levels I_m and $4I_0/\pi Q_p$ are shown by solid and dashed lines.

Our simulations also agree with experiment in that they show little variation in the switching current from trial to trial. Using a 40-μs dwell time, we found no bias points above the tops of the vertical bars shown in Fig. 27 where switching failed to occur and no bias points below the bottoms of the vertical bars where switching occurred. Moreover, the Monte Carlo switching levels do not depend strongly on the dwell time for times greater than about 10 μs. In extending the dwell time from 10 to 20 μs, only marginal changes were noted in the switch points and, in the further extension from 20 to 40 μs, most switch points did not change within the 0.05-nA resolution of our calculation. This insensitivity to dwell time explains why the Monte Carlo results for 40 μs are in good agreement with experiments in which the effective dwell time is orders of magnitude longer.

The agreement between experiment and simulation evident in Fig. 27 assures us that the circuit model of Fig. 2(c) includes all the elements necessary to explain the switching current in junctions that display phase diffusion. The Monte Carlo results do not, however, tell us which elements most directly affect I_s. In Sec. III, we argued that phase diffusion is unlikely to be observed in junctions for which I_s exceeds I_m, and we will show in this section that I_m sets the basic current scale for switching from the phase-diffusion branch. By definition, I_m is the minimum bias for which a junction will switch to the quasiparticle curve in the absence of noise if it is initialized at a potential maximum with an infinitesimal junction voltage and no voltage on the external capacitors. This bias level is significant because it defines the nature of the state-space topology at the saddle point, where escape from a potential well is most likely to occur in the limit of low temperature. For $I<I_m$ the basins of attraction for neighboring wells are contiguous at the saddle point, as in Figs. 9(a) and 14, but for $I>I_m$ the basin of the 1 state intervenes between the basins of neighboring wells, as in Fig. 9(b). Thus, at bias points above I_m, thermally induced escape from a potential well is likely to cause a switch to the quasiparticle branch while, at bias points below I_m, escape will more probably be followed by retrapping.

The bias level I_m, calculated from its definition for the circuit model of Fig. 2(c), is plotted as a solid line in Fig. 27. Because the results for parameters corresponding to samples A and B are nearly identical, only a single curve is drawn for I_m. Although we have argued that I_s should scale with I_m, Fig. 27 shows that I_m is at best a rough approximation to I_s. In the data shown here, I_m exceeds I_s by as much as a factor of 4 and I_m is nearly the same for the two samples, while I_s is distinctly sample dependent. Nonetheless, I_m does increase with temperature above 2 K in a way that mimics a rise in I_s observed for both samples. The fact that I_s increases with temperature is surprising since the increased noise at higher temperatures usually leads to reduced switching currents, as noted in Sec. II. Although the calculation of I_m does not involve noise, it does involve the quasiparticle resistance which decreases with temperature. Thus, assuming that I_s scales with I_m, the observed rise in I_s with increasing temperature can be attributed to a decrease in the quasiparticle resistance.

Further insight into this situation is obtained by considering the estimate $I_m \approx 4I_0/\pi Q_p$ suggested in Sec. III. In evaluating the quality factor at the plasma frequency, $Q_p \equiv R_p(2eI_0C/\hbar)^{1/2}$, we take the shunt resistance to be the parallel combination of the external conductance associated with the isolation resistor, Eq. (48), and the quasiparticle conductance at low voltages, Eq. (44),

$$R_p=[(\omega_p C_s/2R_s)^{1/2}+G_1\exp(-E/kT)]^{-1}\ . \qquad (66)$$

Although the quasiparticle conductance is much smaller than that of the isolation resistor and was neglected in Sec. V, it represents an important correction here because it accounts entirely for the temperature dependence of Q_p. The quantity $4I_0/\pi Q_p$, evaluated using Eq. (66), is plotted as a dashed line in Fig. 27. While $4I_0/\pi Q_p$ approximates I_m only roughly in magnitude, its temperature dependence is nearly identical with that of I_m. Numerical equivalence aside, the approximation $I_m \approx 4I_0/\pi Q_p$ is valuable because it connects I_s directly with the quasiparticle resistance. If I_s scales as I_m which scales as $1/R_p$, then the switching current will be sensitive to the quasiparticle resistance when this resistance is comparable to or smaller than the external shunting resistance at the plasma frequency. For temperatures below 2 K, the quasiparticle resistance is much higher than the 16.4 kΩ resistance presented by the external shunt at the plasma frequency and I_m is nearly constant. As the temperature approaches 4 K, however, the quasiparticle resistance drops to 164 kΩ, decreasing the quality factor and raising I_m slightly. In physical terms, the increased damping at higher temperatures stabilizes the phase-diffusion state and allows it to persist at higher bias levels in spite of the increased noise. A similar explanation for an observed increase in switching current with temperature was previously proposed by Akoh *et al.*[1] and Iansiti *et al.*[3,4]

As these arguments show, I_m can be a useful reference point for understanding the switching current even though it does not accurately estimate I_s. In general, however, I_m tends to overestimate the switching current, as illustrated in Fig. 27. By definition, I_m is the minimum bias at which escape from a potential well through the saddle point causes switching to the quasiparticle branch. That is, I_m applies to a situation in which the potential maximum is reached with no voltage on the junction or the external capacitance, as would occur in the limit of low temperature. However, as discussed in Sec. V, the junction voltage at the point of escape can be significant at the relatively high temperatures of interest here. In addition, phase diffusion leads to an average junction voltage at the switching bias which also appears on the external capacitors. Because I_m neglects the energy stored in the junction and the external capacitors at the point of escape, it usually overestimates the dc bias required for a switch to the quasiparticle branch.

Unfortunately, the energy-storage effects that reduce the switching current below I_m are complicated in the

case of the circuit model that describes our experiment. We can, however, gain further insight into these effects using the simple model with frequency-dependent damping shown in Fig. 2(b). In particular, we consider the case $Q_0=100$, $Q_1=10$, and $\rho=0.1$ for which noise-affected *I-V* curves are shown in Fig. 16. The normalized switching current determined for this case by Monte Carlo simulations is plotted as a function of temperature in Fig. 28. The Monte Carlo results are shown by vertical bars which define the bias range where switching is likely for a dwell time of 10^8 units. In this case, the junction resistance is independent of temperature, so i_m is a constant and i_s decreases monotonically with increasing temperature. We are interested primarily in temperatures between $\Gamma=0.5$ and 4 where phase-diffusion gives the *I-V* curve a finite slope at the origin. In this temperature range, the Monte Carlo results for i_s are generally below $i_m=0.1267$ although the switching current reaches this level at $\Gamma=0.5$. The switching current continues to increase as the temperature is reduced below $\Gamma=0.5$ but phase-diffusion effects are much less important at these low temperatures and at $\Gamma=0.1$ the occurrence of even a single phase slip is unlikely within a dwell time of 10^8 units for all bias points less than i_m. Thus, at temperatures below $\Gamma=0.1$, phase diffusion is absent from the *I-V* curve and we expect to observe switching directly from the zero-voltage state as in the experiments of Fulton and Dunkleberger.[12]

Restricting our attention to temperatures greater than $\Gamma=0.5$, where phase diffusion is fully developed, we now consider how the threshold current for switching to the quasiparticle branch is affected by the initial charge on the junction capacitance C and the external capacitance C_b. Let us define the threshold current $i_t(v_e,v_{be})$ to be the minimum bias at which switching occurs in the noise-free system when the junction is initialized at a potential maximum with a voltage v_e on C and a voltage v_{be} on C_b. This threshold can be evaluated for a given v_e and v_{be} by direct numerical simulation of the circuit dynamics. Numerical results for i_t are plotted as a function of v_e for several values of v_{be} in Fig. 29. By definition $i_t(0,0)$ is equal to i_m and this limit is approached by the $v_{be}=0$ curve of Fig. 29. Positive values of v_e and v_{be} give the system an initial boost toward the quasiparticle branch and thus reduce i_t below i_m. However, because the quasiparticle branch does not exist for bias levels below the zero-temperature return current $i_{r0}=0.0260$, i_t can never be less than this value. Thus, the threshold current decreases monotonically with both v_e and v_{be} but is restricted to the range $i_{r0}<i_t<i_m$.

Given a method for evaluating the voltages v_e and v_{be} at the point of escape, the threshold current can be used to estimate the switching current. For an accurate evaluation of v_e and v_{be}, we turn first to our Monte Carlo simulations. Because a single escape event can cause a switch to the quasiparticle branch, we should, in applying i_t to estimate i_s, adopt the maximum values of v_e and v_{be} that are likely to occur during the dwell time. For simplicity, however, we use instead the average values $\langle v_e \rangle$ and $\langle v_{be} \rangle$, with the anticipation that the computed threshold will overestimate the switching current. Because $\langle v_e \rangle$ and $\langle v_{be} \rangle$ depend on the dc bias, a self-consistent value for i_t can be determined only by trial and error. That is, to find the threshold we must search for a dc bias i such that $i_t(\langle v_e \rangle,\langle v_{be} \rangle)=i$ when $\langle v_e \rangle$ and $\langle v_{be} \rangle$ correspond to the Monte Carlo averages for the given i. Threshold currents determined in this way are plotted as circles in Fig. 28. These values for i_t are in rough quantitative agreement with the i_s values derived from the full Monte Carlo simulations. The fact that i_t provides a much better estimate of i_s than i_m provides, shows that the energy stored in the capacitors C and C_b

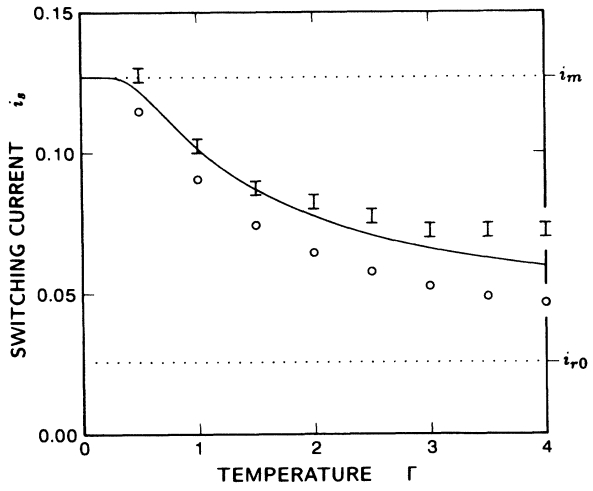

FIG. 28. Switching current as a function of temperature for the circuit of Fig. 2(b) with $Q_0=100$, $Q_1=10$, and $\rho=0.1$. Vertical bars show the results of Monte Carlo simulations, with the bottom of the bar indicating the highest bias point at which switching is not observed during a time of 10^8 units and the top of the bar indicating the lowest bias at which switching is observed within this time. Circles show i_t, the threshold for switching estimated on the basis of Monte Carlo averages for junction and external capacitor voltages at the point of escape. Equation (68) is plotted as a solid line.

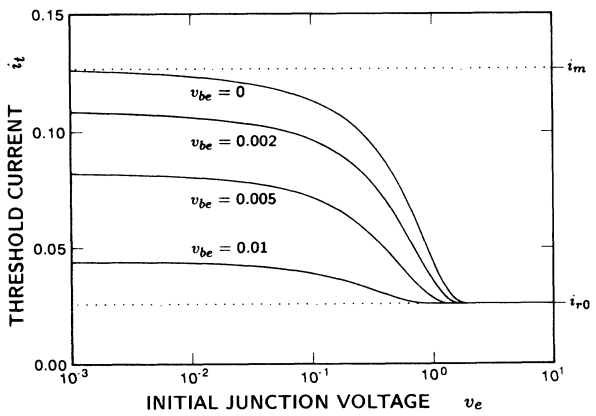

FIG. 29. Threshold current for the circuit model of Fig. 2(b) as a function of initial voltage v_e on the junction capacitor for various values of the initial voltage v_{be} on the external capacitor. The circuit parameters are $Q_0=100$, $Q_1=10$, and $\rho=0.1$.

at the point of escape is important in determining the bias level at which switching to the quasiparticle branch becomes likely.

In using i_t to estimate i_s, we have assumed that the junction is likely to switch to the quasiparticle branch if the system enters the basin of the 1-state attractor. If this assumption were correct, then i_t would be an upper bound on the switching current. However, the approximate values of i_t plotted as circles in Fig. 28 are less than i_s even though these values are overestimates. Thus, our assumption that entering the basin of the 1-state attractor makes switching likely is not always correct. In fact, for the bias point $i=0.08$ just below i_s at $\Gamma=2$, the system must enter the 1-state basin in over half of the 23 000 escape events recorded during the dwell time, since the averages $\langle v_e \rangle$ and $\langle v_{be} \rangle$ are well above the values of v_e and v_{be} required for switching in the noise-free system. Thus, at bias points slightly above i_t, noise can drive the system into the 1-state basin thousands of times without causing a switch to the quasiparticle branch.

This behavior can be understood in terms of the cliff-edge scenario mentioned in Sec. II and the switching dynamics illustrated in Figs. 15(b) and 15(c). As we noted in Sec. II, at bias points just above that for which switching is possible in the noise-free system, i_t in the present case, the switching trajectory hugs the boundaries of the 0-state attractors during the first oscillations down the washboard potential. During this initial period, a small noise pulse can easily cause the system to retrap and prevent the switch to the quasiparticle branch that would have occurred in the absence of noise. Although it might be argued that noise is just as likely to aid the advance toward the 1-state attractor as to cause retrapping, the nonlinearity of the system creates an asymmetry that favors retrapping. The asymmetry results because a switch to the 1-state requires charging the large external capacitance C_b while retrapping requires only that the relatively small junction capacitance C be discharged. The effect of this asymmetry can be seen by comparing Figs. 15(b) and 15(c). In the switch from the phase-diffusion branch to the quasiparticle branch, shown in Fig. 15(b), the average junction voltage rises only very slowly as the external capacitance is charged. In the return process, shown in Fig. 15(c), the junction voltage drops suddenly to zero at the time of retrapping and remains near zero over the much longer time required to discharge the external capacitance. Thus, in the period just after escape, a noise pulse that would have little effect in advancing the system toward the 1-state attractor can, if it has the opposite sign, discharge the junction capacitance and produce a retrapping event that completely stops progress toward the 1 state. Because the time required to charge C_b is long, there is ample opportunity for retrapping to occur and the probability of retrapping can be nearly 1 even for bias levels somewhat above i_t. Indeed, as Fig. 28 shows, the bias level may need to exceed i_t by as much as 50% for retrapping to fail once in 10^4 escape events.

In this discussion, we have identified three corrections, all due to thermal noise, that must be applied to i_m to produce an accurate estimate of i_s for the phase-diffusion branch. First, noise typically supplies more energy than is required for escape and this extra energy reduces the bias required for switching. Second, noise causes phase diffusion which charges the external capacitance and further reduces the switching bias. Third, noise produces retrapping after escape has occurred and this effect increases the switching bias. Of these effects, charging of the external capacitance is most important for the case shown in Fig. 28 and a simple approximate formula for i_s can be derived if we consider this effect alone. Because the time constant for charging and discharging C_b is relatively long, the voltage V_{be} on C_b at the point of escape is always nearly equal to the average phase-diffusion voltage $\langle V \rangle$. The long time constant further implies that the effect of V_{be} will be to supply an additional bias current V_{be}/R_s to the junction during the switching process. Thus, if the bias I_m is the threshold for switching in the absence of a charge on C_b, the threshold in the presence of this charge is approximately

$$I_t = I_m - V_{be}/R_s \ . \tag{67}$$

In dimensionless form this equation becomes $i_t = i_m - v_{be}(Q_0/Q_1 - 1)$, which is well verified by the values of i_t shown in Fig. 29 for small v_e. Equation (67) becomes a formula for the switching current when V_{be} is evaluated at the threshold bias. We noted above that $V_{be} \approx \langle V \rangle$ and, if we approximate the phase-diffusion part of the I-V curve by $\langle V \rangle = IR_0$, we obtain $V_{be} \approx I_t R_0$ at the threshold bias. Combining this result with Eq. (67) yields

$$I_t = \frac{I_m}{1+R_0/R_s} \ . \tag{68}$$

If Eqs. (39) and (65) are used to evaluate I_m and R_0, Eq. (68) becomes an approximate formula for the switching current. Although this formula, plotted as the solid line in Fig. 28, is in good agreement with the Monte Carlo values for i_s, the agreement is partly fortuitous because the error that results from neglecting the curvature in the phase-diffusion branch by assuming $\langle V \rangle = IR_0$ compensates for the omission of retrapping effects. Nonetheless, Eq. (68) clearly accounts for the principal effects determining the switching current in the present instance.

Returning to the experimental case shown in Fig. 29, we briefly reconsider the difference between I_m and the Monte Carlo values of I_s found there. If we attempt to explain these differences in terms of a threshold current I_t that accounts for the effect of energy storage at the point of escape, then I_t will depend on the voltages on the parasitic capacitors C_{si} associated with the series resistance as well as the voltages on C and C_b. Numerical experiments show that the corrections due to these energy storage effects are sufficient to explain the observed difference between I_m and I_s. Unfortunately, I_t is sensitive to all of the several voltages involved and we are unable to derive an approximate formula for the switching current for this case. In particular, there appears to be no simple explanation for the fact that I_s is larger for the sample having the smaller isolation resistance R_s. Because switching involves the time constant $R_s C_b$, as not-

ed in connection with Fig. 15(b), it is not surprising that I_s is sensitive to R_s. We might argue that a small R_s implies a large switching current because I_m scales inversely with the quality factor and Q is smaller for sample B than sample A over a range of frequencies just above $1/R_sC_b$, as shown in Fig. 18. However, other significant effects, such as that described by Eq. (68), give the opposite dependence on R_s. Thus, the relative magnitude of the switching current for samples A and B appears to be the product of several competing effects that can only be resolved through a full Monte Carlo simulation.

Finally, setting aside the complex dynamics that determines the exact switching current, we note that I_m provides an order-of-magnitude estimate for I_s that can be used to set an approximate value for the quality factor at the plasma frequency. Using the approximation $i_m \approx 4/\pi Q_p$ discussed earlier, we estimate that $Q_p \approx 64$ for the present case, based on the fact that the switching current is roughly 2% of the critical current. Although this estimate exceeds the actual Q_p by a factor of 2, a rough estimate such as this could be valuable in many situations, considering the difficulty of measuring the damping at high frequencies.

VII. RETURN CURRENT

The return current I_r is the dc bias at which a junction returns from the quasiparticle branch of a hysteretic I-V curve to the zero-voltage or phase-diffusion branch. Because the return bias varies from trial to trial in the presence of noise, a definite value can in principle be assigned to I_r only if it is defined, like I_s, as an average. However, in the experiments and simulations presented here, the random variations in the return bias are small enough that the statistical nature of I_r can be disregarded.

The return current for samples A and B is plotted in Fig. 30 as a function of temperature. Circles show the experimental values and vertical bars show the results of Monte Carlo simulations based on the circuit model of Fig. 2(c). The experiment and simulation are in excellent agreement, differing by no more than 20% over the range of temperatures studied. Again, we emphasize that this agreement results for entirely nominal circuit parameters.

In order to gain an understanding of the factors that determine the return current, we consider I_{r0}, the return current for the noise-free system. Values for I_{r0}, calculated using the circuit model of Fig. 2(c) with the noise sources set to zero, are plotted as squares in Fig. 30. Comparing I_{r0} with the Monte Carlo results for I_r, we find that the quasiparticle branch extends to lower bias levels in the absence of noise, as expected. Since the noise increases with temperature, the difference between I_r and I_{r0} also increases with temperature and is significant only above 3 K. However, the largest part of the temperature dependence of I_r is accounted for by I_{r0}, which depends on temperature only through the quasiparticle resistance R_J. Thus, Fig. 30 shows that I_{r0} and I_r are both highly dependent on R_J.

A simple formula for I_{r0} appropriate to the case of frequency-dependent damping can be obtained from an approximate I-V curve for the quasiparticle branch that derives from an energy balance relation. For steady-state motion, the energy gained in moving down the washboard potential must equal the energy lost in dissipation. Considering this energy balance over a single Josephson oscillation, we obtain

$$2\pi(I/I_0)E_J = E_d \ , \tag{69}$$

which derives from Eq. (52) in the steady-state limit. In evaluating E_d, the energy loss per oscillation, we make use of the fact that the return event occurs from a finite voltage in the case of frequency-dependent damping. In the limit of high voltage and low damping, we can as-

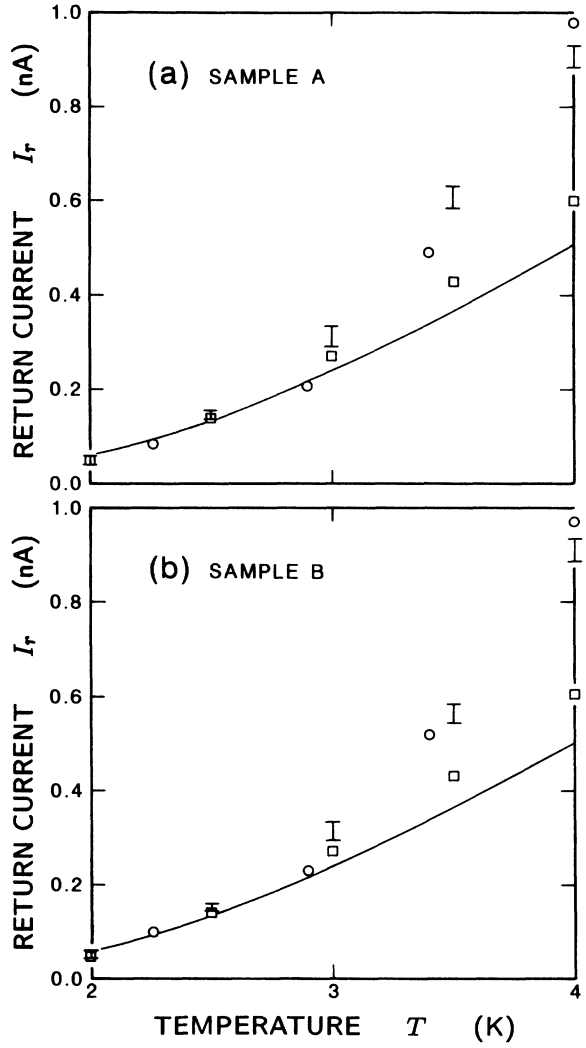

FIG. 30. The return current as a function of temperature for (a) sample A and (b) sample B. Experimental results are shown by circles. Vertical bars show the results of Monte Carlo simulations for the full circuit model shown in Fig. 2(c) including noise. The tops of the bars show the lowest bias point at which a return event was not observed during a 100-μs dwell time and the bottoms show the highest bias point for which a return event was observed within 100 μs. Squares show the noise-free return current I_{r0} computed for the circuit model of Fig. 2(c). Equation (81) is plotted by a solid line.

sume that the voltage waveform is nearly sinusoidal and has the form

$$V=\langle V\rangle+V_2\sin(\omega_J t)\ , \tag{70}$$

where $\omega_J=2e\langle V\rangle/\hbar$ is the Josephson frequency. The current through the admittance $Y(\omega)$ shunting the ideal Josephson element is

$$I_Y=G(0)\langle V\rangle+G(\omega_J)V_2\sin(\omega_J t)+B(\omega_J)V_2\cos(\omega_J t)\ , \tag{71}$$

where $G(\omega)$ and $B(\omega)$ are the real and imaginary parts of $Y(\omega)$. The energy loss per cycle is thus

$$E_d=\int_0^{2\pi/\omega_J} I_Y V\,dt$$
$$=\frac{2\pi E_J}{I_0}[G(0)\langle V\rangle+\tfrac{1}{2}G(\omega_J)V_2^2/\langle V\rangle]\ . \tag{72}$$

To determine the amplitude V_2 of the voltage oscillations, we note that this voltage results from current oscillations of amplitude I_0 in the junction which flow through the admittance Y. In the cases of interest here, $Y(\omega_J)$ is dominated by the admittance of the junction capacitance so that

$$V_2=I_0/\omega_J C_J\ . \tag{73}$$

Combining Eqs. (69), (72), and (73), we obtain

$$I=G(0)\langle V\rangle+\tfrac{1}{2}G(\omega_J)V_p^4/\langle V\rangle^3\quad(\omega_J=2e\langle V\rangle/\hbar)\ , \tag{74}$$

where $V_p=\hbar\omega_p/2e$ is the voltage corresponding to the plasma frequency. This equation specifies the I-V characteristic on the quasiparticle branch in the limit of high voltages ($\langle V\rangle\gg V_p$) for an underdamped junction ($Q_p\gg1$) with a linear shunt admittance. If $G(\omega)$ does not increase faster than ω^3 at high frequencies, the second term of Eq. (74) diverges in the limit of small $\langle V\rangle$. In this case, there is a voltage $\langle V\rangle_{r0}$ below which the I-V curve has a negative slope and there is no stable operating point in this region. The current corresponding to $\langle V\rangle_{r0}$ is the return current I_{r0} of the noise-free system.

We first apply Eq. (74) to determine I_{r0} for the circuit model of Fig. 2(b). Using the fact that $G(\omega)=I_0/V_pQ(\omega)$, we can express $G(0)$ in terms of Q_0 and, assuming that $\omega_J\gg1/R_sC_b$, we can express $G(\omega_J)$ in terms of Q_1 (cf. Fig. 12). In this case, Eq. (74) becomes

$$I/I_0=\frac{1}{Q_0}(\langle V\rangle/V_p)+\frac{1}{2Q_1}(\langle V\rangle/V_p)^{-3}\ . \tag{75}$$

In terms of dimensionless parameters, this equation is

$$i=\langle v\rangle+\frac{1}{2Q_0^3Q_1\langle v\rangle^3}\ . \tag{76}$$

Equation (76) defines an approximate, noise-free quasiparticle branch which is plotted as a dashed line in Fig. 31 for the case $Q_0=5$, $Q_1=2$, and $\rho=0.1$. In this figure, the accurate quasiparticle branch is plotted by a solid line and the return switch points for both curves are marked by circles. The return switch point for the approximate I-V curve is defined by the condition $dI/d\langle V\rangle=0$ which yields

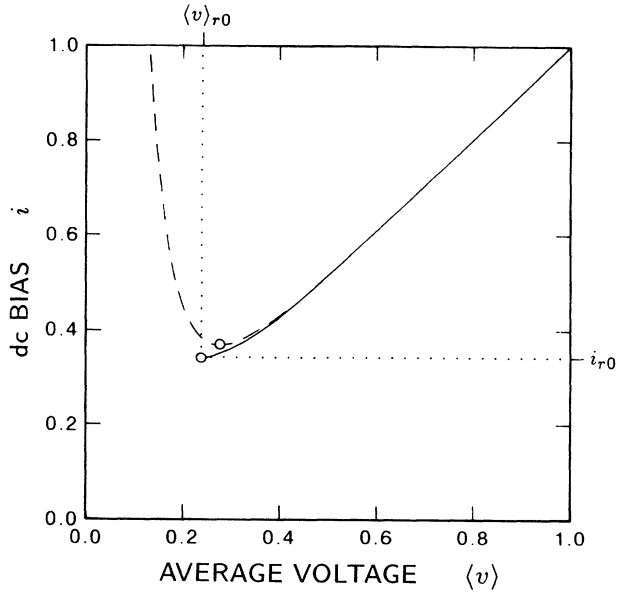

FIG. 31. Quasiparticle branch of the noise-free I-V curve for the junction model shown in Fig. 2(b) with the parameters $Q_0=5$, $Q_1=2$, and $\rho=0.1$. The solid line shows an accurate numerical result and the dashed line shows the approximation given by Eq. (76). For each curve, the point at which the return switch occurs is marked by a circle.

$$\langle V\rangle_{r0}=\left[\frac{3Q_0}{2Q_1}\right]^{1/4}V_p\ , \tag{77}$$

$$I_{r0}=(2^{7/4}/3^{3/4})\frac{I_0}{Q_0^{3/4}Q_1^{1/4}}\ . \tag{78}$$

Because Q_0 is necessarily greater than or equal to Q_1, Eq. (77) shows that the return voltage is on the order of or greater than the voltage corresponding to the plasma frequency. From Eq. (78) we learn that the return current depends primarily on the damping at low frequencies and only weakly on the damping at high frequencies.

In the limit $Q_0=Q_1=Q$ the model of Fig. 2(b) reduces to the RCSJ model, and we might expect Eq. (78) for the return current to reduce to $i_{r0}Q=4/\pi=1.273$. However, we obtain from Eq. (78) $i_{r0}Q=2^{7/4}/3^{3/4}=1.476$. This discrepancy derives from the fact that we assumed a sinusoidal voltage in our derivation of Eq. (78) but the quasiparticle branch extends to zero voltage in the RCSJ model and the waveform is far from sinusoidal at the return point. Equation (78) is much more accurate in cases where $\langle V\rangle_{r0}$ exceeds V_p. For the case shown in Fig. 31, where $\langle V\rangle_{r0}/V_p=1.4$, Eq. (78) yields $i_{r0}=0.371$ in comparison to the accurate result of 0.343. For the case $Q_0=100$, $Q_1=10$, and $\rho=0.1$ considered previously, $\langle V\rangle_{r0}/V_p=2.0$ and the accurate result for i_{r0} is 0.0260 while Eq. (78) yields 0.0262. Thus, Eq. (78) is a good approximation in the limit $Q_0\gg Q_1\gg1$.

To apply Eq. (74) to the experimental case, we must

evaluate the shunt conductance at zero frequency and at frequencies near the plasma frequency. Given the relation $G(\omega)=I_0/V_pQ(\omega)$, this task amounts to reading the correct asymptotes from Fig. 18. While $Q(0)=Q_0$ is simply a constant, its definition requires that we use the asymptotic low-voltage form for the quasiparticle conductance given by Eq. (44). Near the plasma frequency, the shunt conductance is given by Eq. (48) and $Q(\omega)$ is proportional to $1/\sqrt{\omega}$. Thus, we may write $Q(\omega_J)=Q_p\sqrt{V_p/\langle V\rangle}$ and Eq. (74) becomes

$$I/I_0=\frac{1}{Q_0}(\langle V\rangle/V_p)+\frac{1}{2Q_p}(\langle V\rangle/V_p)^{-5/2}\ . \tag{79}$$

Setting $dI/d\langle V\rangle=0$ to solve for the return switch point yields

$$\langle V\rangle_{r0}=\left[\frac{5Q_0}{4Q_p}\right]^{2/7}V_p\ , \tag{80}$$

$$I_{r0}=(7/5^{5/7}2^{4/7})\frac{I_0}{Q_0^{5/7}Q_p^{2/7}}\ . \tag{81}$$

Thus, we find again that the return voltage is on the order of or greater than the plasma voltage and the return current depends more strongly on the damping at zero frequency that at high frequencies.

Equation (81) for the noise-free return current is plotted as a solid line in Fig. 30 where it can be compared with values of I_{r0}, plotted as squares, computed through dynamical simulations. Although there is a significant difference between our analytic result and the simulations, additional calculations show that this difference is largely attributable to the fact that the voltage dependence of R_J was omitted in deriving Eq. (81). The conclusion to be drawn from comparing the squares with the solid line in Fig. 30 is that the curvature in the quasiparticle curve apparent in Fig. 17 produces a modest increase in I_{r0} over what would result if this curve were straight. Thus, Eq. (81) fails to reproduce the experimental results because it omits both the voltage dependence of the quasiparticle resistance and the effects of noise. At temperatures below 3 K, where both of these effects are small, Eq. (81) is in good agreement with both the experimental data and the full Monte Carlo simulations.

Comparing the return current of samples A and B, shown in frames (a) and (b) of Fig. 30, we find no significant difference. Equation (81) suggests an explanation for this coincidence. According to this equation, the return current depends only on the damping at zero frequency and near the plasma frequency. However, as Fig. 18 shows, the damping is the same for both samples at these two frequencies even though there are significant differences at intermediate frequencies. Thus, the coincidence in I_r between the two samples is completely consistent with Eq. (81).

Recently, several authors[44–46] have investigated the return current within the context of the Werthamer model of junction dynamics. This detailed microscopic approach relates the return current to fundamental properties of the superconducting materials. In agreement with the present work, these studies show that I_r is determined largely by the quasiparticle conductance. While we have simply measured this conductance by applying a magnetic field to suppress the Josephson current, the microscopic theories calculate this conductance from first principles. In further contrast to our approach, the microscopic theories treat the junction dynamics using the full Werthamer model rather than the elementary Josephson equations. However, the success of our simple approach to the return current shows that, at least in some cases, it is not necessary to consider the full microscopic dynamics to obtain good agreement with experiment. That is, by basing our calculations of I_r on the measured quasiparticle conductance, we seem to have eliminated all need of the Werthamer model.

Kirtley *et al.*[46] have recently suggested that measurements of I_r can be used to determine the damping of a junction at high frequencies. Our study shows that it would be difficult to obtain an accurate value for Q_p from measurements of I_r. Although I_r certainly depends on the damping at frequencies near ω_p, the examples discussed above show that this dependence is relatively weak, involving $Q_p^{1/4}$ and $Q_p^{2/7}$ in the two cases considered. Moreover, it is necessary to know the frequency dependence of Q in the neighborhood of ω_p in order to determine the relation between I_r and Q_p. Given this uncertainty and the fact that I_r depends more strongly on Q_0 than Q_p, a reliable estimate of Q_p necessarily requires significant information in addition to a knowledge of I_r. A more reliable estimate for Q_p might be obtained from the switching current I_s for the phase-diffusion branch, as suggested in Sec. VI.

VIII. CONCLUSION

We have studied noise-affected *I-V* curves for small-area junctions in which the phase-diffusion and quasiparticle branches overlap each other in their range of dc bias. This overlap implies that two distinct voltage states coexist at some values of dc bias. The low-voltage, phase-diffusion state is associated with slow, diffusive motion in which the system, under the influence of thermal noise, repeatedly escapes from and is retrapped in the local minima of the washboard potential. In contrast, the high-voltage state, corresponding to the quasiparticle branch, is associated with rapid, nearly uniform motion down the slope of the washboard.

The fact that the high- and low-voltage states are stable under the same conditions is surprising because the escape events necessary for phase diffusion might be expected to result in continued acceleration that would take the system to the quasiparticle branch. Indeed, within the simple RCSJ model, this type of switching event is likely at all bias levels for which the high-voltage state is stable, and overlap between the phase-diffusion and quasiparticle branches is not possible. The absence of such overlap in the RCSJ model is related to the fact that the basins of attraction for adjacent potential minima have no common boundary at bias levels for which the high-voltage state is stable. That is, a finger of the basin of the high-voltage state separates the basins of each pair of adjacent minima, and phase-diffusion cannot occur un-

less the system enters the basin of the high-voltage state. Because the probability of switching to the high-voltage state is significant if the system enters its basin of attraction, the phase-diffusion state is unstable in the simple RCSJ model at bias levels where the quasiparticle branch is stable.

However, overlap between the phase-diffusion and quasiparticle branches is possible within an extended RCSJ model in which external loading provides frequency-dependent damping. In particular, if the damping is greater near the plasma frequency than at zero frequency, then there is a range of dc bias $I_{r0} < I < I_m$ for which the basin of the high-voltage state does not intervene between the basins of adjacent potential wells. In this case, the system can escape from a given well under the influence of thermal noise and retrap in a neighboring well without entering the basin of the high-voltage state. Thus, frequency-dependent damping can create a bias region in which both the phase-diffusion and quasiparticle branches are stable.

Although the extent of overlap between the phase-diffusion and quasiparticle branches is dependent on the level of thermal noise, it is roughly defined by the parameters I_{r0} and I_m of the noise-free system. These parameters, in turn, depend on the quality factor Q_0 at zero frequency and the quality factor Q_p at the plasma frequency. Assuming that $Q_0 > Q_p \gg 1$,

$$\frac{I_{r0}}{I_0} \approx \begin{cases} 1.476/Q_0^{3/4}Q_p^{1/4}, & Q(\omega) \propto \omega^0 \text{ for } \omega \geq \omega_p \\ 1.492/Q_0^{5/7}Q_p^{2/7}, & Q(\omega) \propto \omega^{-1/2} \end{cases} \quad (82a)$$

$$\text{for } \omega \geq \omega_p \quad (82b)$$

and

$$\frac{I_m}{I_0} \approx 1.273/Q_p \ . \quad (83)$$

Thus, I_{r0} is largely determined by Q_0 and I_m is largely determined by Q_p. A broad range of overlap between the phase-diffusion and quasiparticle branches ($I_m \gg I_{r0}$) results if $Q_0 \gg Q_p$.

The sensitivity of I_{r0} and I_m to Q_0 and Q_p suggests the importance of understanding loss mechanisms over a broad frequency range in the interpretation of I-V characteristics. In the present work, a good fit between simulation and experiment was obtained only when the losses were accurately modeled at frequencies well into the microwave region. In the case of small-area junctions with a high subgap resistance, an essential element of this model is usually the load represented by the external measuring circuit. Although the impedance of the external circuit may be high at low frequencies, at microwave frequencies it is likely to be on the order of the impedance of free space, unless special precautions are taken. Thus, a detailed understanding of I-V curves for high-resistance junctions is most easily obtained when the external circuit is designed, as in the present experiments, to have a well-defined impedance at microwave frequencies.

The Monte Carlo simulations presented here reveal an aspect of phase diffusion in underdamped junctions not previously noted. In the underdamped case, escape from a potential well often causes the system to move through several potential wells before retrapping occurs. Such multiple-well phase-slip events can have a significant effect on the phase-diffusion resistance R_0 measured at the origin, increasing it in some cases by more than an order of magnitude over predictions based on single-well transitions. A simple model developed here for multiple-well events yields a formula for R_0 applicable to a wide range of situations that is in good agreement with both our Monte Carlo simulations and our experiment.

We have considered small-capacitance junctions similar to those used in the investigation of effects such as SET and MQT which involve phenomena beyond those encompassed by the classical Josephson equations. However, the phenomena discussed here, including hysteresis between the phase-diffusion and quasiparticle branches of the I-V curve, are well described by the classical equations. Although hysteresis of this type is peculiar to small junctions, it derives simply from the fact that, for junctions having a high internal resistance, the damping at microwave frequencies is typically determined by the external loading. We have shown that the external loading can have significant effects, including qualitative changes in the I-V curve. Because such effects are likely to be found in junctions that also exhibit SET and MQT phenomena, our study may serve as a useful stepping stone to understanding these more complex situations.

ACKNOWLEDGMENTS

We are pleased to thank R. L. Mattis and M. Potts for making available unused time on the computers for which they are system managers. This work was supported in part by the U.S. Office of Naval Research under Contract No. N00014-88-F-0077.

[1]H. Akoh, O. Liengme, M. Iansiti, M. Tinkham, and J. U. Free, Phys. Rev. B **33**, 2038 (1986).

[2]R. H. Ono, M. W. Cromar, R. L. Kautz, R. J. Soulen, J. H. Colwell, and W. E. Fogle, IEEE Trans. Magn. **MAG-23**, 1670 (1987).

[3]M. Iansiti, A. T. Johnson, W. F. Smith, H. Rogalla, C. J. Lobb, and M. Tinkham, Phys. Rev. Lett. **59**, 489 (1987).

[4]M. Iansiti, M. Tinkham, A. T. Johnson, W. F. Smith, and C. J. Lobb, Phys. Rev. B **39**, 6465 (1989).

[5]M. Iansiti, A. T. Johnson, C. J. Lobb, and M. Tinkham, Phys. Rev. B **40**, 11 370 (1989).

[6]J. M. Martinis and R. L. Kautz, Phys. Rev. Lett. **63**, 1507 (1989).

[7]W. C. Stewart, Appl. Phys. Lett. **12**, 277 (1968).

[8]D. E. McCumber, J. Appl. Phys. **39**, 3113 (1968).

[9]V. Ambegaokar and B. I. Halperin, Phys. Rev. Lett. **22**, 1364 (1969); **23**, 274 (1969).

[10]M. Simmonds and W. H. Parker, Phys. Rev. Lett. **24**, 876

(1970).
[11]P. A. Lee, J. Appl. Phys. **42**, 325 (1971).
[12]T. A. Fulton and L. N. Dunkleberger, Phys. Rev. B **9**, 4760 (1974).
[13]Y. M. Ivanchenko and L. A. Zil'berman, Zh. Eksp. Teor. Fiz. **55**, 2395 (1968) [Sov. Phys.—JETP **28**, 1272 (1969)].
[14]A. C. Biswas and S. S. Jha, Phys. Rev. B **2**, 2543 (1970).
[15]V. N. Belykh, N. F. Pedersen, and O. H. Soerensen, Phys. Rev. B **16**, 4853 (1977).
[16]H. A. Kramers, Physica (Amsterdam) **7**, 284 (1940).
[17]H. D. Vollmer and H. Risken, Z. Phys. B **37**, 343 (1980); **52**, 259 (1983).
[18]E. Ben-Jacob, D. J. Bergman, B. J. Matkowsky, and Z. Schuss, Phys. Rev. A **26**, 2805 (1982).
[19]P. Jung and H. Risken, Z. Phys. B **54**, 357 (1984).
[20]R. Cristiano and P. Silvestrini, J. Appl. Phys. **59**, 1401 (1986).
[21]R. Graham and T. Tél, Phys. Rev. A **33**, 1322 (1986); **38**, 5944 (1988).
[22]E. Kappos and S. Sastry, in *Proceedings of the 1988 IEEE International Symposium on Circuits and Systems, Espoo, Finland* (IEEE, New York, 1988), p. 1589.
[23]R. L. Kautz, Phys. Rev. A **38**, 2066 (1988).
[24]P. Grassberger, J. Phys. A **22**, 3283 (1989).
[25]M. Büttiker, E. P. Harris, and R. Landauer, Phys. Rev. B **28**, 1268 (1983).
[26]A. Barone, R. Cristiano, and P. Silvestrini, J. Appl. Phys. **58**, 3822 (1985).
[27]V. I. Mel'nikov, Zh. Eksp. Teor. Fiz. **88**, 1429 (1985) [Sov. Phys.—JETP **61**, 855 (1985)].
[28]R. F. Voss and R. A. Webb, Phys. Rev. Lett. **47**, 265 (1981); Phys. Rev. B **24**, 7447 (1981).
[29]L. D. Jackel, J. P. Gordon, E. L. Hu, R. E. Howard, L. A. Fetter, D. M. Tennant, R. W. Epworth, and J. Kurkijärvi, Phys. Rev. Lett. **47**, 697 (1981).
[30]S. Washburn, R. A. Webb, R. F. Voss, and S. F. Faris, Phys. Rev. Lett. **54**, 2712 (1985).
[31]M. H. Devoret, J. M. Martinis, and J. Clarke, Phys. Rev. Lett. **55**, 1908 (1985).
[32]J. M. Martinis, M. H. Devoret, and J. Clarke, Phys. Rev. B **35**, 4682 (1987).
[33]P. Silvestrini, O. Liengme, and K. E. Gray, Phys. Rev. B **37**, 1525 (1988).
[34]P. Silvestrini, S. Pagano, R. Cristiano, O. Liengme, and K. E. Gray, Phys. Rev. Lett. **60**, 844 (1988).
[35]E. Turlot, D. Esteve, C. Urbina, J. M. Martinis, M. H. Devoret, S. Linkwitz, and H. Grabert, Phys. Rev. Lett. **62**, 1788 (1989).
[36]P. Silvestrini and R. Cristiano, Nuovo Cimento **9**, 1433 (1987).
[37]J. Kurkijärvi and V. Ambegaokar, Phys. Lett. **31A**, 314 (1970).
[38]R. F. Voss, J. Low Temp. Phys. **42**, 151 (1981).
[39]M. I. Freidlin and A. D. Wentzell, *Random Perturbations of Dynamical Systems* (Springer, New York, 1984).
[40]R. E. Harris, R. C. Dynes, and D. M. Ginsberg, Phys. Rev. B **14**, 993 (1976).
[41]J. H. Magerlein, IEEE Trans. Magn. **MAG-17**, 286 (1981).
[42]W. L. Stutzman and G. A. Thide, *Antenna Theory and Design* (Wiley, New York, 1981).
[43]*Handbook of Mathematical Functions,* edited by M. Abramowitz and I. A. Stegun (U.S. GPO, Washington, D.C., 1972), p. 297.
[44]H. Kratz and W. Jutzi, IEEE Trans. Magn. **MAG-23**, 731 (1987).
[45]Y. C. Chen, M. P. A. Fisher, and A. J. Leggett, J. Appl. Phys. **64**, 3119 (1988).
[46]J. R. Kirtley, C. D. Tesche, W. J. Gallagher, A. W. Kleinsasser, R. L. Sandstrom, S. I. Raider, and M. P. A. Fisher, Phys. Rev. Lett. **61**, 2372 (1988).

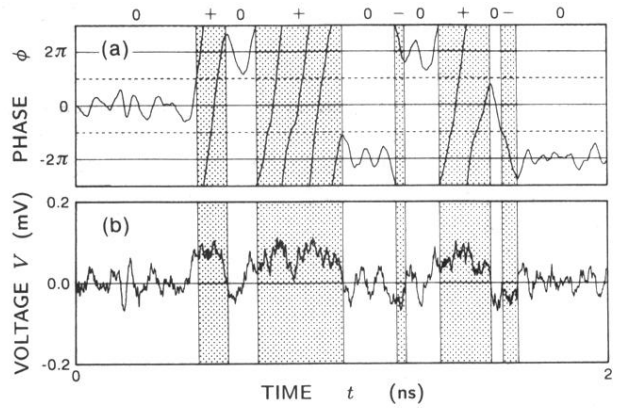

FIG. 20. Calculated time dependence of (a) the phase and (b) the voltage of a junction in the phase-diffusion state corresponding to the experimental situation shown in Fig. 1 for a dc bias of $I = 0.5$ nA. Shaded regions indicate time intervals during which the junction is in the $\pm$ state and unshaded regions correspond to the 0 state.